Reconstructing a Carboniferous inferred coral-alcyonarian association using a biomineralogical approach

Ismael Coronado[a*], Esperanza Fernández-Martínez[b], Sergio Rodríguez[a,c], Francis Tourneur[d]

[a*] Departamento de Paleontología, Universidad Complutense de Madrid, C/José Antonio Nováis 2, Ciudad Universitaria, E-28040 Madrid, Spain. icoronad@ucm.es

[b] Departamento de Geografía y Geología, Facultad de Ciencias Biológicas y Ambientales, Universidad de León, Campus de Vegazana s/n, 24071 León, Spain. e.fernandez@unileon.es

[c] Instituto de Geociencias (IGEO. CSIC-UCM), C/José Antonio Nováis 2, Ciudad Universitaria, E-28040 Madrid, Spain. sergrodr@geo.ucm.es

[d] Pierres et Marbres de Wallonie, ASBL. 11, rue des Pieds d'Alouette. B-5100 Naninne, Belgium. francis.tourneur@pierresetmarbres.be

Abstract

The taxonomic assignation and ecological implications of the genus *Syringoalcyon* Termier & Termier, 1945 have been a palaeontological problem for a long time. Carboniferous material from Morocco and Spain has been studied using a biomineralogical approach by means of petrographic microscopy, SEM, AFM, EMPA and CIP microscopy analysis. Detailed morphological, structural, chemical composition and crystallographic data enable a deeper understanding of the nature of *Syringoalcyon*. The coral walls and the so-called epithecal scales exhibit conspicuous differences in microstructure (lamellae and holacanthine fibres in the coral versus single crystal in scales), nanostructure (pill-shaped versus granule-shaped nanocrystals), composition (LMC versus HMC) and crystallographic orientation. The results of these analyses imply that *Syringoalcyon* is an association between the tabulate coral *Syringopora* and an epibiont. They also suggest that the epibiont was an alcyonarian (a rare occurrence in the fossil record) that was attached to the syringoporoid. This work highlights the utility of the biomineralizational approaches for solving palaeontological problems, such as systematic affinities, and for advancing knowledge of the evolution of biocrystallization processes.

INTRODUCTION

New palaeontological perspectives can be gained from in-depth studies of biomineralization in recent and fossil organisms (Lloyd *et al*., 2008; Raven & Giordano, 2009; Jackson *et al*., 2010). Comparisons between recent and fossil organisms allow new insights into the formation of skeletal elements through the geological record (Porter, 2010; Cuif *et al*., 2011; Sabbatini *et al*., 2014). This knowledge offers an opportunity to establish the systematic affinities of problematical fossils by the study of their biomineralogical features (geochemical signature, crystalline structures and crystallographic properties). Additionally, these studies can shed light on the evolutionary processes of formation of biominerals through Earth's history.

The problematical genus *Syringoalcyon* Termier & Termier, 1945 was originally erected based on a single specimen from the Viséan (Lower Carboniferous) of central Morocco, assigned to *Syringoalcyon maroccanum*. It consists of a colony composed of vertical tubes of syringoporoid coral morphology but with the addition of numerous monocrystalline scales with their apices directed upwards and densely arranged around the external wall of each corallite. According to Termier & Termier (1945, 1975): 1) the scales belong to the same organism as the rest of the skeleton, and 2) this organism could belong to either Alcyonaria or Porifera.

Young & Noble (1987) studied a single corallum of *Syringopora bifurcata* Lonsdale (Tabulata) from the Silurian of New Brunswick (Canada) which includes some scales that are "almost identical" to those described by Termier & Termier (1945, 1975). The authors interpreted these "epithecal scales" as encrusting organisms of unknown affinities and considered the genus *Syringoalcyon* to be a junior synonym of *Syringopora* (Goldfuss, 1826).

Tourneur *et al*. (1995) revised the original material of *Syringoalcyon* and the colony of *Syringopora bifurcata* described by Young & Noble (1987) using petrographic sections, cathodoluminescence and electron microprobe analysis (EMPA). These researchers supported the interpretation of the scales as the skeletons of epibionts of uncertain biological affinities.

Apart from the type-species, *Syringoalcyon maroccana*, three other species have been assigned to this genus within the Palaeotethys: *S. dobrolyubovae* Tchudinova, 1986 (Aktyubinsk Region, Southern Urals; upper Sakmarian-lower Artinskian); *S. unicum* Tchudinova, 1986 (Novotroitsk, Akkermanovka central quarry, southern Urals; Serpukhovian) and *S. tchudinovae* Ogar, 1992 (Tien-Shan, Viséan).

The occurrence of epithecal scales similar to those described in *Syringoalcyon* has also been cited in several genera of tabulate and rugose corals both from the Silurian and Lower Devonian (cited in Shurigina, 1972 and Ogar, 1992).

This paper is a biomineralogical study of the Carboniferous genus *Syringoalcyon* based on structural, crystallographic and chemical compositional data. The aim of this study is to find biomineralogical criteria to 1) distinguish the scales from the coral’s skeleton, 2) provide evidence for the taxonomic assignment of the scale maker, and 3) interpret the possible role of the scales.

MATERIAL AND METHODS

The material studied in this research is in the collection of the Universidad Complutense of Madrid (Spain) and consists of two specimens:

A fragment of the topotype specimen described by Termier & Termier (1975) from the Viséan of Tizi ben zizouit, Dchar Aït Abdallah region, north-eastern part of the

Moroccan Meseta called “Massif Central”. Label DPM 00782 SYR01, nine thin sections and two ultra-thin sections.

A sample from the Viséan of Fuenteobejuna (Ossa-Morena region, SW Spain). Label DPM 00782 SYR02, two thin sections and two ultra-thin sections.

To identify and evaluate the relationship between the coral and the scales, a combination of different structural and chemical techniques, including petrographic microscopy, scanning electron microscopy (SEM), atomic force microscopy (AFM), electron microprobe analysis (EMPA) and cathodoluminescence (CL) were undertaken at the Universidad Complutense, Madrid (Spain). In order to understand the crystallographic differences between the coral wall and the scales, computer-integrated-polarization microscopy (CIP) was employed (for details of this technique see Coronado *et al*., 2014). A detailed description of these methods can be found in the supporting information.

RESULTS

Petrographic microscopy revealed three basic elements: tabulate coral (genus *Syringopora*), scales and matrix.

The structural study of the calcitic elements (coral wall and scales) was subdivided into different parts depending on the scale of the work. Microstructural characterisation includes the data obtained with petrographic microscopy and SEM from the coral wall and scales, whereas nanostructural characterisation includes the data obtained by AFM from the coral wall, scales and echinoderm plates for comparison.

Petrographic description

Tabulate coral

Syringopora is the type genus of the family Syringoporidae whose main features have been discussed by Tchudinova (1986) and Young & Noble (1987). The following description is based on the specimens studied in this paper. A more precise systematic study will be addressed in a forthcoming paper.

The corallum is massive-fasciculate and composed of cylindrical corallites (Fig. 1), connected by transverse stolons (or tubes). Inside the corallites two main structural elements can be found: tabulae (sometimes forming an axial tube) and septal spines.

Scales

The main feature of *Syringoalcyon* is the occurrence of abundant, small, 340 µm (300 – 413 µm), upwardly directed, crook- or scale-shaped structures attached to the outer walls of the corallites (Fig. 1). These epithecal scales usually cover the entire wall of each corallite and the upper parts of the transverse stolons, but they never exceed the highest part of the coral calyx (Figs. 1B, F). Dense stacking of scales occur in tangential sections of the coral (Fig. 2B and 2C).

In longitudinal section, the scales are crook-shaped; in cross-section, they are ellipsoidal when cut at their widest part, or linear if the cut is in the more distal, narrow part. In tangential sections they show an ellipsoidal or sub-rhomboidal outline.

Matrix

Because the specimens studied in this paper come from two locations and different facies, the matrix surrounding them is varied, although some elements occur in all the studied samples: sparite patches, automicrite, micropeloids and micrite coating.

Material from Morocco: Packstone composed of micropeloidal micrite, microdolomite and patches of sparite. Quartz crystals of sub-rounded or sub-rectangular outline are present. The matrix-supported bioclastic elements show micrite coatings and evidence of corrosion. The main skeletal elements are transported and they consist of crinoids, bryozoans, brachiopods and foraminifers.

Material from Spain: This matrix is a skeletal grainstone and micropeloidal wackstone. It is mainly composed of micropeloidal micrite and patches of sparite, in which *Thartarella* burrows (Coronado & Rodríguez, 2010) commonly occur.

Microstructure

Petrographic microscopy and SEM show that the coral wall microstructure is formed by lamellae (*sensu* Lafuste, 1983). The calcite crystals are straight to slightly wavy, with indentations at their edges, flake forms and are completely imbricated with each other showing a compact packaging (Fig, 2B and D). These structures have a lateral development in two dimensions, with lengths from 9.04 to 39.53 µm (x = 20.25 µm; n = 60), and widths from 2.09 to 5.05 µm (x = 3.25 µm; n = 60).

Holacanth septal spines (composed of fibres) are very closely spaced in transverse section and irregularly spaced in longitudinal section. They are long and thin and have a significant development towards the lumen of the coral. In the wall, the occurrence of strong wavy features is usual (Fig. 2B) and these are the result of the gradual accommodation of the lamellae around the spines (in both development and direction), passing gradually from lamellae to fibres (Fig. 2D).

The scales around the coral walls have a single crystal structure that is evident in both SEM and petrographic images. Both techniques show that the contacts between the scales and the lamellae are not gradual, as in the transition of fibres to lamellae of the coral wall. The scales inserted into the wall. They show a basal zone that is flat or slightly convex, 75 µm in size and 58 µm in depth, which is surrounded by coral lamellae (Fig. 2A and E). These lamellae are truncated and/or broken. The region of contact of the basal zone of the scale with the coral wall, in the area of insertion, sometimes shows a loss of lamellar microstructure (Fig, S2). The insertion area shows a region that is sub-granular in petrographic images and cloudy in SEM images (Fig. 2E). This insertion shows a footstep-shape towards the outside of the corallites (Figs. 2A and E). Some gaps (depth = 50 µm) occur in areas with loose scales. In slightly tangential sections, the scales overlap and gaps are present.

The scales have a turbid texture (cloudy appearance) due to the occurrence of abundant micro-inclusions, which can be opaque or translucent (Fig. 2A). According to their size and location, two regions can be distinguished in each scale: 1) an external fringe or cortex where small inclusions (size 0.53 to 1.26 µm) occur (Fig, S2B); and 2) an inner region or core where large inclusions (size 3.3 to 6.9 µm) are developed (Fig, S2B). The core starts at the basal region (just at the point of insertion into the coral wall) and growth is towards the apex, whereas the cortex surrounds the core from the edge of the coral wall at the footstep-shaped region (Fig. 2A, S2B).

SEM images show that the inclusions have a sub-angular to sub-rounded morphology and are occasionally filled with crystals (Fig. 2F). The habit and chemistry of these crystals (known from EDX system and EMPA) suggest that they are dolomite. The complete dissolution of the sub-rounded impurities and the resulting pierced plane suggest that they were preserved via dissolution of a previous element.

The scale surfaces show some knobs or protuberances, which are usually disposed along the edges of a crystal (Fig. 2A).

Nanostructure

Atomic force microscopy (AFM) has previously been successfully used to observe the original nanostructure of calcite skeletons of the tabulate coral *Multithecopora hontoriense* (Syringoporicae, Coronado *et al*., 2013) and other fossils such as scleractinians (Stolarski & Mazur, 2005) and molluscs (Dauphin, 2002). Coronado *et al*. (2013) found that the nanotexture of *Multithecopora hontoriense* is maintained in all of the structural elements (fibres and lamellae) as a stacking of rod-shaped nanocrystals, co-oriented in the same structural element. Based on this finding, an AFM study of the coral walls, scales, and echinoderm plates was designed for comparison. (Fig. 3A).

The AFM images of the coral wall (Fig 3B-D) show at low-scale magnification that there is a preserved nanotexture, which is composed of granular nanocrystals that form rows and are co-oriented.

A detailed view of the contact between two lamellae shows that the nanogranules are pill-shaped and co-oriented to the short side of the lamella (c-axis). This is more clearly visible in 3D images (Fig. 3D). In phase images, the edges of these pill-shaped crystals have a dark colour, thus indicating that they have a different composition, e.g., that the crystals are not uniform (Fig. 3C). Some authors (Dauphin, 2002; Cuif *et al*., 2008; Gorzelak *et al*., 2013) have studied similar envelopes in Recent and fossil organisms and suggested that they could be organic linings from the original organic matrix. The poor preservation of this dark coloured lining in the coral wall of the current study could indicate that nanogranules became partially merged during diagenesis.

The size of the nanocrystals is variable and strongly dependent on the microcrystal cut. Pill-shaped crystals show lengths that vary between 46 nm and 146 nm (x = 80 nm, N = 25) and their width fluctuates between 31 and 49 nm (x = 40 nm, N = 25).

The scales show flat regions where pseudo-nanocrystals appear to be completely merged and the original textures have been obliterated (Fig. S3A-B) and some other regions (tens of microns across) that exhibit a visible nanotexture. In these latter areas, height images reveal that the single crystal structure is composed of co-oriented nanofibres, while phase images show nanogranules with a dark coating. High-magnification images reveal that these fibres are formed by subunits of granule-shaped nanocrystals (Fig 3E-I). These subunits are well-rounded and agglomerated in large units (fibres) around 200 nm in length (Fig. S3C), which have a common orientation in rows, as is seen in the 3D image (Fig. 3G; Fig. S3D). The sizes of the nanocrystals are not as variable as in the coral wall. Well-rounded, granule-shaped crystals show a length that varies between 35 nm and 59 nm (x = 47 nm, n = 25) and a width between 24 and 31 nm (x = 28 nm, n = 25).

As in the scales, the echinoderm plates have large regions that are completely flat, thus indicating an obliterated nanotexture; these occasionally have the same morphology as that of rhombohedral dolomite crystals (Fig. S3E-F). Small areas (tens of microns) even show a visible nanotexture, although evidence of merger is present. In the areas where the nanotexture is preserved, the echinoderm plates also have granule-shaped nanocrystals with irregular morphologies and sizes and do not show a preferential orientation. Phase images reveal that the nanogranules have a dark, although not marked, coating suggesting the occurrence of residual organic matrix. Rounded granule-shaped crystals show a length that varies between 26 nm and 70 nm (x = 47 nm, n = 25) and width between 21 and 60 nm (x = 33 nm, n = 25).

The length and width of each crystal has been represented in a scatter plot showing that the nanocrystals of the coral wall have larger sizes and show a greater dispersion than those of the scales and the echinoderm plates (Fig. S4). The crystal sizes of the scales and the echinoderm plates are quite similar, although the nanocrystals of the scales show a smaller dispersion.

Chemical composition

EMPA mapping (Fig. 4) of ten elements (Ca^{2+}, Mg^{2+}, Sr^{2+}, S^{6+}, Ba^{2+}, Na^{+}, Mn^{2+}, Fe^{2+}, Al^{2+} and Si^{2+}) from sample DPM 00782 SYR01 was performed to evaluate the chemical composition of the scales and the coral wall. In the backscatter electron image (BSE) and the petrographic micrograph (Fig. 4L), two longitudinal sections of scales showing insertion into the coral wall (Fig. 4A, left) and the surrounding matrix can be observed. The brightness (grey-scale) of the BSE image depends mainly on the atomic number of elements at each point. Four main regions can be distinguished in the BSE image (coral wall, scale, insertion-edge of coral wall zone and matrix, Fig. S5). The BSE image of the sample shows some microstructural details of scales including the cortex with impurities (Fig. S5A, S2B), the different shaded pattern at the insertion zone and the large and black impurities in the scale's core. In this BSE image the coral wall is characterised by a homogeneous shade in which the lamellar frame is visible.

Levels of Ca^{2+} and Mg^{2+} (Figs. 4B-C) are quite homogeneous in the coral wall, except for isolated spots. In contrast, the scales have variable amounts of Ca^{2+}, being more uniform towards the apex of the scale (Fig. 4B). In those zones where there are microcrystals, the Ca^{2+} concentrations are even lower but the Mg^{2+} is higher. These crystals, or spots, with high Mg^{2+} are concentrated at the insertion regions of the scales and scattered in an isolated manner at the edge of the coral wall. The increase in Ca^{2+} in the regions surrounding these crystals and the high amount of Mg^{2+} in these zones indicate that they are microdolomite crystals. On the other hand, EMPA mapping shows high Mg^{2+} concentrations surrounding the scales and at the edge of coral wall, which match with the presence of a micritic coating (Fig. 4L).

Sr^{2+} and Na^{2+} are homogeneous except in some silicate crystals of the matrix (Figs. 4G, K). Similarly, Ba^{2+} has a homogeneous distribution in the coral wall and depletion in the scales, with a high concentration at the edges of the scales and in the matrix (Fig. 4J). In addition, Fe^{2+} and Mn^{2+} have a uniform distribution in the coral wall. In the scales, there are places (the edge of crystals, some altered regions) where the Fe^{2+} is more abundant and that matches the bright zones in the BSE image. Furthermore, the Mn^{2+} concentration is uniform in both the coral wall and scales and is at lower levels than in the matrix. Al^{2+} and Si^{2+} have been mapped to highlight the areas with silicate minerals (Figs. 4F, I). The distribution of these elements coincides both in the matrix, and in the micritic coating surrounding the scales; it also coincides with Ba^{2+} distribution (Fig. 4J). Finally, there are places where the amounts of aluminium are higher and they correspond with the spots with impurities in the zone of contact between scale-coral walls and the interior of the scales. Most likely, these facts can be explained as the result of recesses that became contaminated with alumina powder during the polishing process.

Interestingly, S^{6+} exhibits a homogeneous distribution in the coral wall and in the micritic coating around the scales. In previous studies, the content of S^{6+} in skeletons and shells was interpreted as a substitution of SO^{4-} groups for CO^{3-} (Grossman *et al.*, 1996; Dickson, 2001), suggesting an inorganic origin of this element. More recently, it has been shown that S^{6+} is organic in origin and most likely belongs to the SO^{4-} groups of sulphate polysaccharides and the S amino acids of the organic matrix (Cuif *et al.*, 2003; Cuif & Dauphin, 2005; Cusack *et al.*, 2008). Finally, there are isolated spots in the scales where the amount of S^{6+} is higher than in other parts. These spots, viewed under a petrographic microscope and in BSE images, match with micro-impurities in the scales (both core and cortex), which do not have a high concentration of Al^{2+}, suggesting a point concentration of organic molecules.

In addition, 261 point analyses were performed on the coral wall, scales and echinoderm plates for comparison. The values of EMPA were normalised to mol % of $CaCO_3$, $MgCO_3$, $SrCO_3$, $MnCO_3$ and $FeCO_3$. The values of S^{6+}, Na^{2+} and Ba^{2+}, were given as ppm. Table S1 summarises the EMPA analyses for the three elements that were selected, representing the mean, standard deviation (S.D.), minimum, maximum and median.

All analyses in the coral wall show a homogeneous composition with little spatial variation (Fig. 5A). Two transverse lines of different corals were analysed and plotted together, to check for internal variation within the wall. The Mg^{2+} / Ca^{2+} values in the coral show a linear correlation (R^2=0.876) and these elements are located at the same spaces in the lattice of $CaCO_3$. The variation of these elements depends on different processes, with uptake of other elements (such as Sr^{2+} or Ba^{2+}) replacing the Mg^{2+} during coral growth or by alteration of calcite during diagenesis, replacing the Mg^{2+} with Fe^{2+} and Mn^{2+} (Barbin, 2013; Coronado et al., 2013). The mean value of $CaCO_3$ in the coral is 95.47 mol % and cross-sections toward the wall show flat tracks (i.e. a homogeneous composition) according to these values. At the inner edge of the coral wall (just some microns near the calcitic cement), the $CaCO_3$ exhibits slight depletions while the $MgCO_3$ show small increases. The opposite can be seen at places close to the scale insertion points, where the values of Ca^{2+} increase while those of Mg^{2+} decrease. These places also show a strong increase of the Fe^{2+} and Mn^{2+} values.

Most likely, these areas were altered by fluid flow at the contact between the wall and the scales. These elemental patterns match with the data provided by EMPA mapping. The $MgCO_3$ mean value in the corals is 3.97 mol % (Table S1), close to the lower limit of high magnesium calcite (HMC), at 4 mol % of $MgCO_3$. Twelve points have values higher than 4 mol %, all of them being points of alteration zones at the inner edge of the wall or in the insertion zones of the scales.

The amounts of $MgCO_3$ in the different components are compared using box charts (Fig. 5B-C). The mean and median values are similar in all, but the maximum and third quartile of the data has HMC values in the scales. The occurrence of microdolomite inside the scales (as determined by SEM, BSE and EMPA mapping and HMC values from punctual analyses) indicates that they could be composed of HMC. Echinoderm plates are composed of HMC (Dickson, 2001, 2004; Lowenstam and Weiner, 1989) and the BSE images show microdolomite and celestine inclusions scattered in the stereome of the echinoderm plates in our material (Fig. S5C). Therefore, the HMC values of scales and echinoderm plates were plotted in comparison with the low magnesium calcite (LMC) values of the coral wall. Echinoderm plates have higher values than the scales, rising to 10.49 mol %. The mean, S.D., minimum, maximum and median values are summarised in Table S2. Both components exhibit similar values of the mean and median, but the echinoderm values are slightly higher than those of the scales. On the other hand, the mean values of $SrCO_3$ for the coral wall, scales and echinoderm are similar. The differences among the three components lie in the range of variations, with the echinoderm plate having lower and more restricted values than the scales.

CL images were taken with the purpose of evaluating and correlating the geochemical data provided by EMPA. Several kinds of luminescence were observed in the three main components analysed here (coral wall, scales and matrix). The luminescence of the coral wall is null (NL) or dull (DL) depending of the area, being brighter in the wall edges, in the insertion areas of scales and in some isolated points (Fig. S6, S7). In contrast, the scales are mainly luminescent (L) in the core and DL in the cortex, although this result depends on the preservation state of the scales. Those scales that have micritic coatings exhibit a bright luminescence in the external part (Fig. S7c-d), whereas those showing dull luminescence have magnesium contents similar to those occurring at the coral wall (Fig. 4C). Luminescent microcrystals in the inner part of some scales correspond with dolomite crystals and confirm the data provided by the EMPA maps (Fig. 4C). Other scales have a DL or NL in the inner part of the apex (Fig. S6 c-d; S7a-b) but they show low and homogenous contents of magnesium in the outer parts.

On the other hand, matrix and cements exhibits several kinds of luminescence depending of their composition. The micritic areas have a dull luminescence brighter that those showed by the coral wall. The quartz grains have not luminescence and the diagenetical micro fractures, and some sparitic rims of lumen cement have a bright luminescence (Fig. S7). Some isolated crystals of dolomite of the matrix show a high luminescence, similar to those observed in the inner part of scales (Fig. S6a-b).

Crystallographical features

Three c-axis orientation images (COI) and their corresponding pole-figures were obtained using the CIP method from different parts of two ultra-thin-sections. This analysis was performed to determine the crystallographic correlation between the scales and the coral wall (Fig. 6). The petrographic micrograph shows the wavy structure of the lamellae (L) adapting to the development of a septal spine (S). The orientation image shows three main colour regions (green, yellow and dull magenta). The lamellar region shows an orientation of the c-axis perpendicular to their morphological axis in the azimuth and slightly tilted approximately 60° to the growth direction in inclination (Figs. 6D-E). The septal spine is represented by the same colours but more intense than the lamellae in the centre of the wavy region. Unlike the lamellae, their fibres have the c-axis oriented parallel to the morphological axis and show a tilting of approximately 50° and an orientation rotated nearly 30° with respect to the lamellae. This corresponds to the orientation of the septal spine toward the growth of the coral. The morphological axis and therefore the c-axis of those lamellae forming the spine flanks turn around the septal spine. Consequently, their c-axis becomes rotated by 45° in the azimuth and the inclination became analogous to those of the septal spine fibres.

The scales are arranged tangentially to the coral wall. The petrographic micrograph shows the interruption and truncation of lamellar growth and the incorporation of lamellae into the scale (Fig. 6A, white arrows). The orientation of the c-axis of the scales is represented by dull colours, which means a very upright orientation of the c-axis in the standard colour look-up table (CLUT), as can be seen in the pole figure and the selected regions (Fig. 6E).

Figure S8 represents a longitudinal section of *Syringopora* showing the place where scales insert into the coral wall, and the basal zone with a step-shaped path in the widest region. The petrographic micrograph shows that the lamellae are cut in the insertion zones. The lamellar region has a well-differentiated orientation in the c-orientation images (Fig. S8C). Green, yellow and dark magenta colours indicate a c-axis orientation that is perpendicular to the morphological axis, and the inclination is at low angles (35° to 60°, depending on the section), in contrast to Fig. 6 where the lamellae have a greater inclination to the pole maxima. A slight wavyness of the lamellae is observed in the coral wall and the variation of the c-axis is the broadest (Fig. S7E).

Diagenetic alteration can be mapped with CIP because during the process of dissolution/co-precipitation the original crystallographic orientations are lost, even if the microstructure is preserved (Pérez-Huerta *et al.*, 2007, 2011, 2012; Coronado *et al.*, 2013, 2015; and Moreno-Azanza *et al.*, 2013). In polycrystalline and well-structured skeletons, as is the case of those with carbonate-controlled biominerals (e.g., corals, molluscs, brachiopods, egg-shells, which have a great crystallographic control), the crystallographic orientations are random after diagenesis. This premise could be applied to the c-axis orientations in the CIP method (Coronado *et al.*, 2014). SEM images of insertion zones show that these regions have lost the microstructure and the EMPA and CL data show diagenetic alteration (Fig. 4, S6, S7). Orientation images show that these cloudy zones have random orientations, which confirm that they are affected by diagenesis. These regions are part of a track of alteration from the external wall toward the lumen, in which some lamellae zones show varied orientations.

Moreover, the scales exhibit a wide range of c-axis orientations. It can be observed that the scales mostly have a magenta colour but some are yellow and orange. Magenta scales represent tangential sections in which the c-axis is sub-parallel to the morphological axis (with an inclination of 60° – 70°, Fig. S8E). Instead, yellow and orange scales are not oriented regarding to the morphological axis. The alteration patterns can be observed in the scales at the lower right corner of the orientation image (Fig. S8E), where the orientation changes inside affecting the adjacent scale. Internally, the scales show small sub-angular micrometric zones where the orientation of the axis is different from the scale orientation. These zones correspond to microdolomite inclusions.

A tangential section of the coral wall (Fig. 7) shows the classical egg-box structure produced by the curvature of lamellae surrounding the septal spines. In the edge of coral wall can be observed the insertion of longitudinal scales and others slightly rotated and cut by them. Two main orientations of scales occur in both pole figures and c-axis orientation images. One shows a dull magenta colouration (E1) and the other displays a dull green colouration (E2). The variation of these orientations is due to the rotation of the morphological axes of the scales. Although the azimuth is preserved during the development of the scale, which is sub-perpendicular to the morphological axis, the inclination varies internally. This variation is preserved at all scales analysed, being approximately 30° from the basal zone to the apex (Fig. 7A-D). This variation could also be seen in the extinction patterns in the petrographic micrograph (Fig. 7E).

DISCUSSION

Before discussing in depth the previously described mineralogical and structural features, it is important to clarify if the scales have or have not preserved their original properties.

AFM studies show that the scales are partially nano-recrystallized. This means that although the microstructure is preserved, the nanocrystals have experienced dissolution-precipitation partially obliterating the original nanostructure, as can be observed by the merger of crystals and the loss of dark coatings (Fig. S3A-B). Similar results have been obtained by Cuif (2014) in fossil Rugosa and Scleractinia. These recrystallization patterns are also observable by CIP, because some scales show diagenetic alteration patterns (Fig. S9), resulting in different orientations of the c-axis. A dull blue colour indicates an inclination similar to other scales and is representative of a concordant c-axis (but rotated, because this is a transverse section of the scale). In other areas of this scale, the original orientation of c-axis (blue dull regions) is obliterated by an alteration pattern (recrystallization front, dull yellow colour), which has a different orientation (almost orthogonal). Euhedral crystals, most likely of microdolomite and calcite, show blue and deep red colours and a random orientation pattern in the pole figure (Fig. S9).

The co-existence of original and altered areas can be explained if the processes of dissolution-precipitation occur as a slow transformation at both nano and molecular scales. HMC is metastable in non-marine diagenetic environments (Ross, 1991). Fluids dissolve HMC and precipitate LMC by Mg^{2+} ion flux, preserving the c-axis orientation and the original micro-morphology. For this process to occur, the new growth or precipitation of calcite should be epitaxial, thus preserving some islands of original information (including crystallo-chemical features). This type of process has been observed in echinoderm skeletons (Oti *et al.*, 1989; Dickson, 2001).

Data from previous analyses have shown strong differences between the scales and the coral wall. These differences are mainly related to the following factors:

Size: The scales are larger than any other element known in Palaeozoic corals.

Microstructure continuity: The coral wall is characterised by a framework composed of skeletal elements (lamellae and fibres), which behave as a continuous structure. The microcrystalline elements change gradually between the different morphologies, adapting their c-axes progressively. The gradual accommodation of microstructural elements is essential (Lafuste, 1978; Coronado *et al.,* 2013) in Palaeozoic corals. However, in *Syringoalcyon* the contact between lamellae and scales is abrupt, showing cut and truncated lamellae, even in some partially altered places. This abrupt change cannot be explained by pressure-dissolution processes produced during diagenesis, because this contact show the typical footstep-shape in all scales independent of their position in coral walls whereas other skeletal elements of the matrix do not show this feature.

Another distinctive feature of the scales is their inner microstructure composed of a cortex and a core, which can be easily differentiated regardless of diagenetic alteration. These two components have never been previously recognized in Palaeozoic corals.

Nanostructure: In spite of diagenesis, the nanostructures of scales and coral wall are observables although they show visible signs of alteration. The nanostructural arrangement suggests that the microcrystals are biocomposite co-oriented, similar to those described by Coronado *et al.* (2013) and Coronado et al. (2014). The nanostructural elements of the scales have different shapes and sizes (Fig. S3) in regard to coral walls.

Mineralogy: The coral wall is LMC with a null luminescence or dull luminescence except for some altered crystals located at the wall edges that show a variable composition and a bright luminescence. In contrast, the scales are LMC, having some regions where the original nanotexture is preserved and HMC remains. Additionally, the presence of microdolomite and patterns of depletion of Mg^{2+} with respect to Ca^{2+} can explain the LMC formation as can be seen in EMPA maps and CL images.

Crystallography: The coral wall is characterized by a crystallographic arrangement similar to this known in other Syringoporicae and in which the *c*-axis has a direction from the external part of the corallite towards the lumen, always parallel to fibres and perpendicular to lamellae. This arrangement is consistent with the co-orientation of the nanocrystals observed using AFM (Fig. 3D). In the transverse section, the c-axes of the lamellae point to the lumen and are slightly tilted to the growth direction, whereas in longitudinal section, the c-axis is even more perpendicular to the coral wall, and the tilting is lower (Coronado *et al.,* 2013, 2014, 2015). Coronado *et al*. (2015) describe the growth mechanisms of this superfamily of tabulate corals from the crystallographic study of the generation of calices; the growth direction is divided into two main components, a horizontal growth direction towards the lumen and a vertical direction towards the outside. In contrast, the scales have a variable *c*-axis orientation and its direction is from the footstep-shape insertion area towards the apex, a pattern that has never been described before in Syringoporicae.

Although some cnidarian (*e.g.* Hydrozoa and Gorgonacea, Lowenstam and Weiner, 1989) have been described with two polymorph minerals (calcite and aragonite) in their skeletons, their occurrence is located in different anatomical parts, which depend on the taxa (Lowenstam, 1964; Cairns and Macintyre, 1992). In addition, they always occur in the same crystalline element forming the skeletons (*e.g.* fibres), so they are integrated in the microstructure. The generation of crystalline elements with polymorphs in different parts of the skeleton, lacking a morphological continuity and showing various crystallochemical properties requires a differentiated mineralizing tissue, as happens in molluscs (Cuif *et al*., 2011). These tissues and processes have never been described in cnidarians. According to these data, *Syringoalcyon* should not be considered as a bi-mineral organism and the scales should have an origin different from that of the *Syringopora* coral wall.

Young & Noble (1987) and Tourneur *et al*. (1995) interpreted these scales as belonging to an epibiont. The results of our study support this interpretation and go a step further by providing evidences about the biological affinities of this epibiont.

Biological affinities of the epibiont

The firsts attempts to identify *Syringoalcyon* were made by Termier & Termier (1945) who linked this genus (and not just the scale maker) to Stolonifera (Alcyonaria), and then to Porifera or to Alcyonaria (Termier & Termier, 1975). Tourneur *et al*. (1995) considered the scales to be the product of an organism of uncertain biological affinities. To date, no further attempts have been made to clarify the systematic position of the scale maker.

The occurrence, size, single crystal appearance on the micro-scale and HMC mineralogy of the scales are features that fit several Palaeozoic invertebrate groups bearing scales or large crystals, mainly Echinodermata, Porifera and Alcyonaria.

The occurrence in the matrix among the corallites of sparitic patches, micropeloids, automicrite and *Thartharella* burrows point to the former presence of organic material in these places. The ichnogenus *Thartharella*, probably generated by a polychaete annelid, is often observed where some type of soft tissue (e.g., sponges and large bacterial mats) occurs (Krainer *et al*., 2003; Coronado & Rodríguez, 2009), most likely because they provide a nutrient source for the tracemaker. Thus, the occurrence of these elements and the absence of scales in the core of the voids among the corallites suggest that a soft-tissue organism occupied the spaces (Fig. 8). This feature allows us to reject organisms with articulated skeletons (echinoderms), which had been taken in account because of the morphology and indented edges of the scales.

Related to HMC Porifera skeletons, the morphology and distribution of hexactinellid spicules are quite different from the scales described in this paper.

The occurrence of a soft body and the HMC mineralogy and morphology of the scales match the features of Alcyonaria (or Octocorallia), a group of Cnidaria with polyps bearing eight tentacles. Alcyonaria also show mineralised tissues, many constituted of different types of spicules or sclerites (Cuif *et al*., 2011). The taxonomy of this group is mainly based on the morphology of their spicule associations and has been quite difficult to apply in fossil organisms (Bengtson, 1981; Chatterton *et al*., 2008). Although there is no agreement on the first record of the octocorals: Cambrian (Ausich & Babcock, 1998; Taylor *et al*., 2013), Early Ordovician (Cope, 2005), Silurian (Bengtson, 1981) or even Ediacaran (McMenamin, 1998), the earliest known spiculate alcyonarian is *Atractosella*, from the Llandovery-Wenlock of Gotland (Sweden).

Nevertheless, most alcyonarian fossils are from the Cretaceous and Cenozoic (Bayer, 1956; Nudds & Löser, 2001).

The alcyonarian-calcified elements (spicules or holdfasts, in some Gorgonacea) consist for the most part of HMC, and in some few cases of aragonite and hydroxyapatite (Cuif *et al.*, 2011). The precise shape of each spicule is specific, although within a species the shape varies according to the anatomical site where it grows, suggesting that the processes of spicule formation are well controlled (Lowenstam & Weiner, 1989). The spicules in alcyonarians are produced in cellules (scleroblasts) in ectodermal-endodermal layers of mesoglea. This growth begins in the vacuole of the scleroblast, which contains organic matrix as a template and can be completed in the extracellular environment, enclosing great amounts of organic matrix into the spicule (Kingsley, 1990). For this reason, during the biocrystallization process the number of black bodies (intracellular vesicles) inside the scleroblast increases (Majoran, 1987).

The spicules are formed by long, joined fibres (Dauphin, 2006; Cuif *et al.*, 2011), which are organised into concentric layers representing successive stages of growth (Majoran, 1987; Dauphin, 2006). AFM study indicates that calcareous fibres are formed of nodular micro-domains. Phase images show nanometric elements with grain-shapes (Dauphin, 2006; Cuif *et al.*, 2011). Schmidt (1924) studied the structural organisation of alcyonarian spicules under polarised light and described four types of c-axis orientations that match with different morphologies. Bengtson (1981) summarised the four morphologies of alcyonaria spicules (spindle-shaped sclerites; spindle or rod-shaped or tuberculated sclerites; rounded or scale-shaped sclerites and spindle-shaped turberculated sclerites).

The scales presented herein match the features of alcyonarian spicules. AFM data show that the scales consist of bundles of sub-micrometre fibres (200 nm in width) oriented parallel to the c-axis development similar to those described by Dauphin (2006). Large magnification areas show that the fibres consist of well-rounded granules of 47 nm length that look like the nodular micro-domains described by Cuif *et al.* (2011) in alcyonarian spicules. The c-axis is perpendicular to the morphological axis and changes along the crystal up to the apex, a fact that explains the undulose extinction observed under polarised light. The spindle-shaped spicules of alcyonarians have a c-axis oriented perpendicular to its morphological axis (Majoran, 1987) and the morphology and ornamentation of *Syringoalcyon* scales is similar to those of the spindle-shaped sclerites (Figs. 8A-D).

Assuming the scales of the epibiont belong to Alcyonaria, we may use the current knowledge of the controlled biocrystallization process of Recent alcyonarians in order to infer how the scales were produced in the past. For this purpose, some observations can be especially useful. At nanoscale, a fibrous arrangement with a stepped-growth mode and co-oriented elements is observed (Figs. S3C-D). At microscale, the development of a cortex non-integrated into the insertion area is seen. The impurities causing the cloudy appearance of scales show a different size in the cortex (where they are smaller) than in the core (where they are larger). According to these observations, the nucleation of scales would be produced inside a scleroblast located in an ectodermal layer and their growth would start in a zone close to the coral wall, probably in an extra-cellular environment. The acid conditions of this contact area would dissolve the lamellar skeleton of the host coral and cause insertion into the coral wall. Furthermore, this growth would produce a cloudy cortex (resembling the concentric layered pattern of alcyonarians). In fossil scales the impurities could be a reflection of alcyonarian black bodies.

Taxonomical and palaeoecological implications of the genus *Syringoalcyon* will be studied in depth in a forthcoming paper highlighting the importance of alcyonarian-tabulate coral association in the Palaeozoic seas.

CONCLUDING REMARKS

Cuif *et al*. (2011) stated that the study of biomineralization is critical to understanding the events of biological evolution, relationships between fossil and Recent groups and the use of biomineral materials as geochemical proxies. Some biomineral features (i.e. structure to micro- and nanoscale, crystallographic properties, geochemical signature of organic and inorganic phases) are characteristics of these groups through time, as occurs in brachiopods, molluscs and corals, among others (Dauphin, 2002; Stolarski & Mazur; 2005; Pérez-Huerta *et al.,* 2007; Porter, 2010). Different groups share some of these characteristics as they arise from a common biocrystallization process and thus these features act as a unique fingerprint of their journey through life. Besides, Mann (2001) established that the biominerals have some properties which are characteristics regarding their inorganic counterpart (as chemical compositions, crystallography, structures, mechanical properties and so on; as, for instance, in the case of nacre, trilobite calcitic lens or otoliths). These specific properties facilitate the identification of biogenic structures in the fossil record and their comparison with other organisms or biomineralization strategies (Jackson *et al.,* 2010; Cuif *et al.,* 2011; Sabbatini *et al.*, 2014). The present paper summarises the main differences between the biominerals forming the coral wall of *Syringopora* and those constituting the scales of the epibiont that habited in the waters of Palaeotethys. Even being partially altered, the distinctive biomineral-characteristics of the scales have permitted to establish a systematic affinity of these remains with the Alcyonaria. This means that, like other groups (Stolarski & Mazur, 2005; Porter, 2010; Cuif *et al*., 2011), the biocontrolled-features of the alcyonarian skeletal elements have kept recognizable properties through the fossil record. This fact means that biomineralization studies must be used as a complementary tool in palaeontology.

Acknowledgements

Financial support through the Spanish *Ministerio de Economía y Competitividad* (research project CGL2012-30922BTE) and Complutense University Research Group (910231) is gratefully acknowledged. Ismael Coronado acknowledges financial support through a FPI-UCM grant and the Synthesys grant FR-TAF-2397 developed in MNHN (Paris, France) during 2012, which allowed to study the material of *Syringoalcyon* from Termier's collections. This research is a contribution to the *IGCP* Project *596. Climate change and biodiversity patterns in the Mid-Palaeozoic*. We also give our sincere thanks to Ian D. Somerville (UCD) for his advices and the English revision of the manuscript.

REFERENCES

Ausich WI, Babcock LE (1998) The phylogenetic position of *Echmatocrinus brachiatus*, a probable octocoral from the Burgess Shale. Palaeontology, 41, 193-202.

Balthasar U, Cusack M, Faryma L, Chung P, Holmer LE, Jin J, Percival IG, Popov LE (2011) Relic aragonite from Ordovician–Silurian brachiopods: Implications for the evolution of calcification. Geology, 39, 967-970.

Bayer FM (1956) Octocorallia. In: Treatise on Invertebrate Paleontology, Part F, Coelenterata (ed R.C. M). Geological Society of America, Boulder, CO, and University of Kansas Press, Lawrence, KS, pp. 497.

Barbin V (2013) Application of cathodoluminescence microscopy to recent and past biological materials: a decade of progress. Mineralogy and Petrology, 107, 353-362.

Bengtson S (1981) *Atractosella*, a Silurian alcyonacean octocoral. Journal of Paleontology, 55, 281-294.

Bruckschen P, Oesmann S, Veizer J (1999) Isotope stratigraphy of the European Carboniferous: proxy signals for ocean chemistry, climate and tectonics. Chemical Geology, 161, 127-163.

Chatterton BDE, Copper P, Dixon OA, Gibb S (2008) Spicules in Silurian tabulate corals from canada, and implications for their affinities. Palaeontology, 51, 173-198.

Cope JCW (2005) Octocorallian and hydroid fossils from the Lower Ordovician of Wales. Palaeontology, 48, 433–445.

Coronado I, Pérez-Huerta A, Rodríguez S (2013) Primary biogenic skeletal structures in *Multithecopora* (Tabulata, Pennsylvanian). Palaeogeography, Palaeoclimatology, Palaeoecology, 386, 286-299.

Coronado I, Pérez-Huerta A, Rodríguez S (2014) Computer-integrated polarisation (CIP) in the analysis of fossils: a case of study in a Palaeozoic coral (Sinopora, Syringoporicae, Carboniferous). Historical Biology, 1-15.

Coronado I, Pérez-Huerta A, Rodríguez S (2015) Crystallographic orientations of structural elements in skeletons of Syringoporicae (tabulate corals, Carboniferous): implications for biomineralization processes in Palaeozoic corals. Palaeontology, 58 (1), 111-132.

Coronado I, Rodríguez S (2009) Análisis de microfacies de los montículos de la Formación Cosgaya. Sección de Las Ilces, Pensilvánico, Cantabria/Microfacies analysis of the Cosgaya Formation mounds. Las Ilces Section, Pennsylvanian, Cantabria, N Spain. Coloquios de Paleontologia, 59, 61-91.

Coronado I, Rodríguez S (2010) Bioacumulación de Filosilicatos en las paredes de un Micro-Burrow de gusano del Carbonífero.Macla. Macla, 13, 67-68.

Cuif J-P, Dauphin Y (2005) The two-step mode of growth in the scleractinian coral skeletons from the micrometre to the overall scale. Journal of Structural Biology, 150, 319-331.

Cuif J-P, Dauphin Y, Doucet J, Salome M, Susini J (2003) XANES mapping of organic sulfate in three scleractinian coral skeletons. Geochimica et Cosmochimica Acta, 67, 75-83.

Cuif J-P, Dauphin Y, Sorauf JE (2011) Biominerals and fossils through time, Cambridge University Press, Cambridge; New York.

Cuif JP, Dauphin Y, Farre B, Nehrke G, Nouet J, Salomé M (2008) Distribution of sulphated polysaccharides within calcareous biominerals suggests a widely shared two-step crystallization process for the microstructural growth units. Mineralogical Magazine, 72, 233-237.

Cusack M, Dauphin Y, Cuif J-P, Salomé M, Freer A, Yin H (2008) Micro-XANES mapping of sulphur and its association with magnesium and phosphorus in the shell of the brachiopod, *Terebratulina retusa*. Chemical Geology, 253, 172-179.

Dauphin Y (2002) Fossil organic matrices of the Callovian aragonitic ammonites from Lukow (Poland): location and composition. International Journal of Earth Sciences, 91, 1071-1080.

Dauphin Y (2006) Mineralizing matrices in the skeletal axes of two Corallium species (Alcyonacea). Comparative Biochemistry and Physiology Part A: Molecular & Integrative Physiology, 145, 54-64.

Dickson JAD (2001) Diagenesis and Crystal Caskets: Echinoderm Mg Calcite Transformation, Dry Canyon, New Mexico, U.S.A. Journal of Sedimentary Research, 71, 764-777.

Dickson JAD (2004) Echinoderm Skeletal Preservation: Calcite-Aragonite Seas and the Mg/Ca Ratio of Phanerozoic Oceans. Journal of Sedimentary Research, 74, 355-365.

Gorzelak P, Stolarski J, Mazur M, Meibom A (2013) Micro- to nanostructure and geochemistry of extant crinoidal echinoderm skeletons. Geobiology, 11, 29-43.

Grossman EL, Mii H-S, Zhang C, Yancey TE (1996) Chemical variation in Pennsylvanian brachiopod shells; diagenetic, taxonomic, microstructural, and seasonal effects. Journal of Sedimentary Research, 66, 1011-1022.

Jackson DJ, Thiel V, Wörheide G (2010) An evolutionary fast-track to biocalcification. Geobiology, 8, 191-196.

Kingsley RJ (1990) Calcium Carbonate Spicules in the Invertebrates. In: Skeletal Biomineralization: Patterns, Processes and Evolutionary Trends. Vol. I. American Geophysical Union, pp. 27-33.

Krainer K, Flügel E, Vachard D, Joachimski MM (2003) A close look at Late Carboniferous Algal Mounds, Schulterkofel, Carnic Alps, Austria. Facies, 49, 325-350.

Lafuste J (1978) Modalites de passage des lamelles aux fibres dans la muraillede Tabules (Micheliniidae) du Devonien et du Permien. Geobios, 11, 405-408.

Lafuste J (1983) Passage des microlamelles aux fibres dans le squelette d'un Tabulé “michelinimorphe” du Viséen du Sahara algérien. Geobios, 16, 755-761.

Lowenstam H, Weiner S (1989) On biomineralization, Oxford University Press, New York.

Lloyd JR, Pearce CI, Coker VS, Pattrick RaD, Van Der Laan G, Cutting R, Vaughan DJ, Paterson-Beedle M, Mikheenko IP, Yong P, Macaskie LE (2008) Biomineralization: linking the fossil record to the production of high value functional materials. Geobiology, 6, 285-297.

Majoran S (1987) Structural investigations of octocoral sclerites. Zoologica Scripta, 16, 277-287.

Mann S (2001) Biomineralization: Principles and concepts in bioinorganic materials chemistry, Oxford University Press, Oxford.

McMenamin MAS (1998) The garden of Ediacara. Discovering the first complex life, New York, NY.

Moreno-Azanza M, Mariani E, Bauluz B, Canudo JI (2013) Growth mechanisms in dinosaur eggshells: an insight from electron backscatter diffraction. Journal of Vertebrate Paleontology, 33, 121-130.

Nudds JR, Löser H (2001) The fossil cnidarian record. In: Proceedings of the 8th International Symposium on Fossil Cnidaria and Porifera, Sendai, Japan. Bulletin of the Tohoku University Museum (ed Ezaki Y, Mori, K., Sugiyama T., Sorauf J.E.), pp. 7-33.

Ogar VV (1992) Discovery of the tabulate genus *Syringoalcyon* in the Lower Carboniferous of Tien Shan. Paleontologicheskii Zhurnal, 0, 110-112.

Oti MN, Ogbuji LU, Breuer KH (1989) Diagenetic transformation of magnesium calcite in a monocrystalline rock-forming carbonate skeleton of an echinoderm. Chemical Geology, 76, 303-308.

Pérez-Huerta A, Cusack M, England J (2007) Crystallography and diagenesis in fossil Craniid brachiopods. Palaeontology, 50, 757-763.

Pérez-Huerta A, Dauphin Y, Cuif JP, Cusack M (2011) High resolution electron backscatter diffraction (EBSD) data from calcite biominerals in recent gastropod shells. Micron, 42, 246-251.

Pérez-Huerta A, Cusack M, Méndez CA (2012) Preliminary assessment of the use of electron backscatter diffraction (EBSD) in conodonts. Lethaia, 45, 253-258.

Porter SM (2010) Calcite and aragonite seas and the de novo acquisition of carbonate skeletons. Geobiology, 8, 256-277.

Raven JA, Giordano M (2009) Biomineralization by photosynthetic organisms: Evidence of coevolution of the organisms and their environment? Geobiology, 7, 140-154.

Ross DJ (1991) Botryoidal high-magnesium calcite marine cements from the Upper Cretaceous of the Mediterranean region. Journal of Sedimentary Research, 61, 349-353.

Sabbatini A, Bédouet L, Marie A, Bartolini A, Landemarre L, Weber MX, Gusti Ngurah Kade Mahardika I, Berland S, Zito F, Vénec-Peyré MT (2014) Biomineralization of *Schlumbergerella floresiana*, a significant carbonate-producing benthic foraminifer. Geobiology, 12, 289-307.

Schmidt WJ (1924) Die bausteine des tierkörpers in polarisiertem lichte, F. Cohen, Bonn.

Shurigina MV (1972) Podklass Tetracoralla, Kishechnopolostnye i brakhiopody zhivetskikh otlozheniy vostochnogo sklona Urala. Izdatelstvo "Nedra"; Moskva. (in Russian).

Stanley SM (2006) Influence of seawater chemistry on biomineralization throughout phanerozoic time: Paleontological and experimental evidence. Palaeogeography, Palaeoclimatology, Palaeoecology, 232, 214-236.

Stolarski J, Mazur M (2005) Nanostructure of biogenic versus abiogenic calcium carbonate crystals. Acta Palaeontologica Polonica, 50, 847-865.

Stolarski J, Meibom A, Przenioslo R, Mazur M (2007) A Cretaceous Scleractinian Coral with a Calcitic Skeleton. Science (New York, N.Y.), 318, 92-94.

Taylor PD, Berning B, Wilson AA (2013) Reinterpretation of the Cambrian “Bryozoan” *Pywackia* as an Octocoral. Journal of Paleontology, 87, 984-990.

Tchudinova II (1986) Composition, System alld Phylogeny of Fossil Corals. Order Syrlngoporida. Trudy Paleontologicheskogo Instituta Akademia Nauka SSSR, 216, 3-77.

Termier H, Termier G (1945) Sur la presence de spicules chez quelques Alcyonaires viséens du Maroc. Société Géologique France, Comptes Rendus, Séances, série 5, 15, 70-72.

Termier H, Termier G (1975) Nouvelles données sur le tabulé énigmatique *Syringoalcyon* Termier et Termier 1945. Geologica et Palaeontologica, 9, 85-93.

Tourneur F, Boulvain F, Young GA (1995) Reinterpretation of *Syringoalcyon* Termier & Termier 1945 (Tabulata); syringoporid coral with epibionts. In: VII Int. Symp. On Fossil Cnidaria and Porifera. Madrid, september 12-15, pp. 92-93.

Young GA, Noble JPA (1987) The Llandovery-Wenlock Syringoporidae from New Brunswick, Canada. Journal of Paleontology, 61, 268-283.

Figure Captions:

Fig. 1. Macroscopic features of *Syringoalcyon*. A-C. Specimen DPM 00782 SYR01. A. Transverse section. Matrix, most likely micritic or microsparitic in origin, is currently dolomitised. Sparitic patches between corallites, micritic coatings around bioclasts and scales have been preserved. B. Longitudinal section showing the scales arranged around the corallites but no to growing in advance of the calices. Note the dense stacking of scales over a stolon (white arrow). C. Detail of a transverse section showing the entry of the scales into the coral wall. Note the occurrence of large bioclasts with micritic coatings and a dolomitised matrix with abundant quartz D-F. D. Transverse section showing the patchy arrangement of the sparite, and the occurrence of micropeloidal-micrite, micritic coatings around the bioclasts and *Thartharella*. E. Longitudinal section showing the void between two corallites of *Syringopora*. Note the scales pointing to the central space, which is filled by sparite. F. Detail of the scales just over a connecting tube showing their insertions into the coral wall. Th: *Thartharella*. Mp: Micropeloids. S: scales.

Fig. 2. A-C. Ultrathin-section images from Syringoalcyon, sample DPM 00782 SYR01. A. Detail of scales and their insertion (yellow arrow) into the coral wall. White arrow shows the basal zone. B. Transverse section of *Syringoalcyon* showing a transverse cut of the scales. Yellow arrow points to the protuberances of the surface. C. Tangential section of *Syringoalcyon* showing a dense stacking of ellipsoidal scale sections. Yellow arrow shows the classical egg-box structure usually seen in the walls of the coral *Syringopora*. D_F. SEM images from *Syringoalcyon*, sample DPM 00782 SYR02. D. Longitudinal section of *Syringopora*. White arrow shows the gradual change between lamellae and fibres in contact with a septal spine. Yellow arrow shows the lamellar microstructure of a tabula. E. Contact between scales and coral wall. Yellow arrows

show the step-shaped insertion area. White arrow shows the external cortex in the scales. F. Detail of the microstructure of a scale. Note the angular raised microdolomite crystals and the total dissolution of impurities showing a pierced plane.

Fig. 3. A. Thin-section image of the areas of *Syringoalcyon* studied by AFM from the sample DPM 00782 SYR01. B_D. AFM images of the coral wall. B. Height image of the longitudinal section of a lamella. C. Phase image of B, where pill-shaped nanocrystals are observed. Note the contact with the adjacent lamella and the transverse cut of the nanocrystals. D. Three-dimensional AFM image of nanocrystals of *Syringopora* coral wall in contact with other lamella. The red arrow shows the direction of the *c*-axis. E-I. AFM images of a scale. E. Phase image where granule-shaped nanocrystals are observed. Note the agglomeration of well-rounded large units and the lineation in the nanofibres. F. Height image of (E) image where the co-orientation of the nanocrystals is observed. G. Three-dimensional AFM image of nanocrystals of the scales. Red arrow shows the direction of the *c*-axis. H,I. Phase and height images of the nanogranules which make up the nanotexture of the scales. Note the dark coating around the crystals. J-L. AFM images of a echinoderm plate. J. Phase images displaying evidences of nano-recrystallisation. Note the merging of nanocrystals at the bottom of the image. K,L. Phase and height images showing more details of the original nanotexture of the echinoderm plate.

Fig 4. *Syringoalcyon* EMPA mapping. A. Specimen DPM 00782 SYR01. BSE image showing the contact between the scales and the coral wall. In the insertion zone, note the different colour between the scale and the coral wall. B-K. Mapping of different elements (Ca^{2+}, Mg^{2+}, Fe^{2+}, Mn^{2+}, Al^{2+}, Sr^{2+}, S^{6+}, Si^{2+}, Ba^{2+} and Na^{+}). L. Thin-section image of the studied area. Note the micritic coatings around the scales located at the edge of the coral wall.

Fig. 5. A. Chart showing the distribution of the amounts of the major elements (Ca^{2+} and Mg^{2+}) along two transverse lines across the coral walls and from different corallites (DPM 00782 SYR01). B. Box-chart showing the amount of $MgCO_3$ in the three investigated components. C. Box-chart showing the amount of $MgCO_3$ in the three studied components, but just plotting the HMC values for the epibiont scales and echinoderm plates.

Fig. 6 *Syringoalcyon*, sample DPM 00782 SYR01. CIP images and the derived *c*-axis pole figures of a transverse section of *Syringoalcyon* and the area of insertion of the scales. A,B. Ultra-thin section image of the investigated area. A. Large magnification image. B. Yellow frame shows the studied area and its position in the coral wall. C. Orientation image of the studied area. Black regions belong to the thick region of contact between the crystals and opaque impurities and they were not considered for the *c*-axis pole figure calculation. D. Pole figure of the entire investigated area calculated as an orientation distribution function and provided in multiples of uniform distribution intervals of 0.5 for *c*-axis orientations. Standard colour look-up table (CLUT) in the lower region. E. Pole figures of some areas studied in detail and superimposed to the whole pole figure. Red points correspond to the punctual *c*-axis orientation of each pixel. L-region belongs to the lamellar zone in the wavy area. S-region belongs to the septal spine region. Note the rotation of the *c*-axis of 45° in relation to the lamellar region. E1 and E2-regions belong to different epibiont scales.

Fig. 7 A-C and H. *Syringoalcyon*, specimen DPM 00782 SYR01. CIP images and derived *c*-axis pole figures of a tangential section of *Syringoalcyon* where the scales are inserted. A. Ultra-thin section image showing the investigated area. B. Orientation image of this area. Black regions belong to regions of thick contact between crystals and opaque impurities and they were not considered for the *c*-axis pole figure calculation. C.

Pole figures of different areas where a more detailed study was achieved superimposed to the whole pole figure. Red points correspond to the punctual *c*-axis orientation of each pixel. E1 and E2-regions belong to different scales. L1 and L2-regions belong to a zone composed of lamellae. H. Pole figure of the whole area calculated as an orientation distribution function, given in multiples of uniform distribution intervals of 0.5 for *c*-axis orientations. Standard colour look-up table (CLUT) in the lower region. D-G. Three-dimensional sketches showing a reconstruction of the scales. Note the texture caused by protuberances.

Fig. 8 Life reconstruction of *Syringoalcyon*, composed of tubes of the tabulate coral *Syringopora* and an unknown alcyonarian that occupies the voids among the corallites.

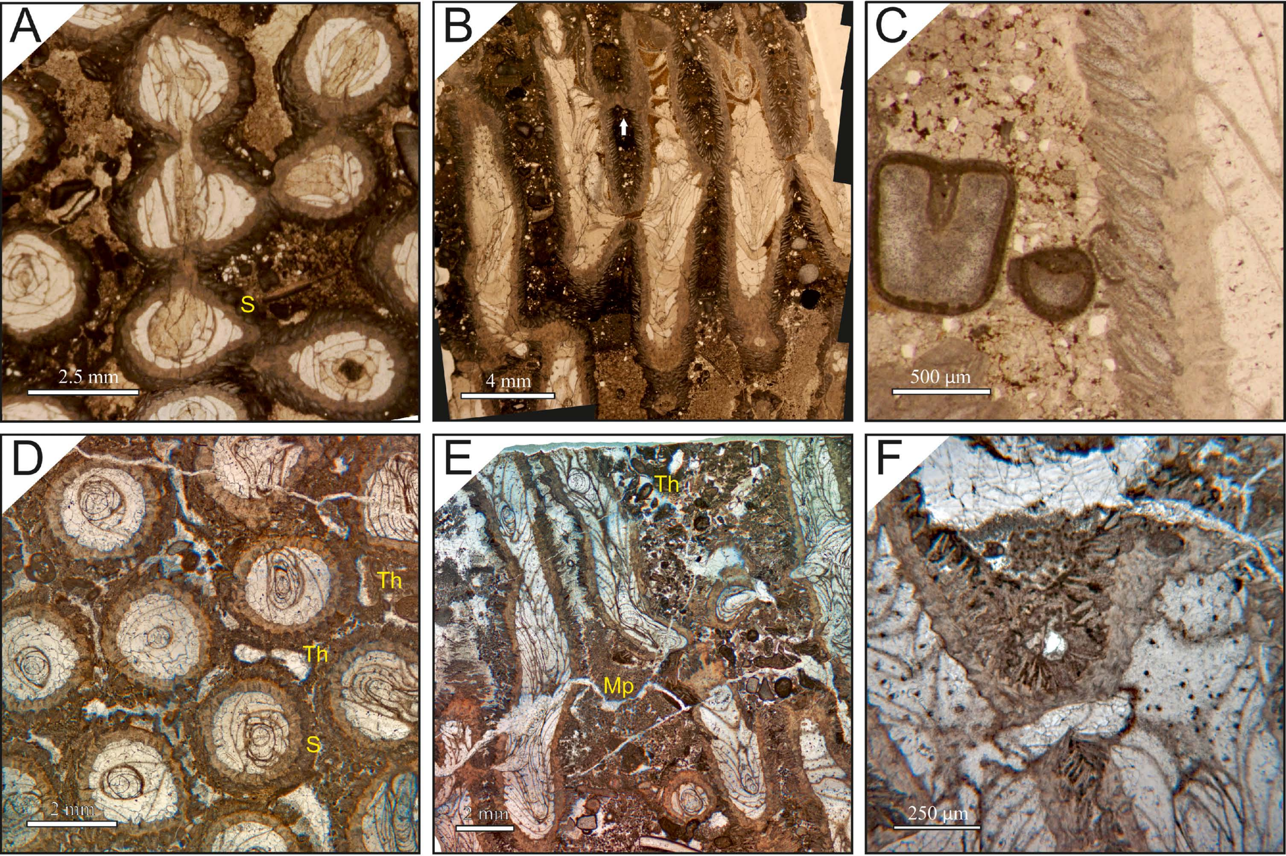
A
S
2.5 mm
B
4 mm
C
500 µm
D
Th
Th
S
2 mm
E
Th
Mp
2 mm
F
250 µm

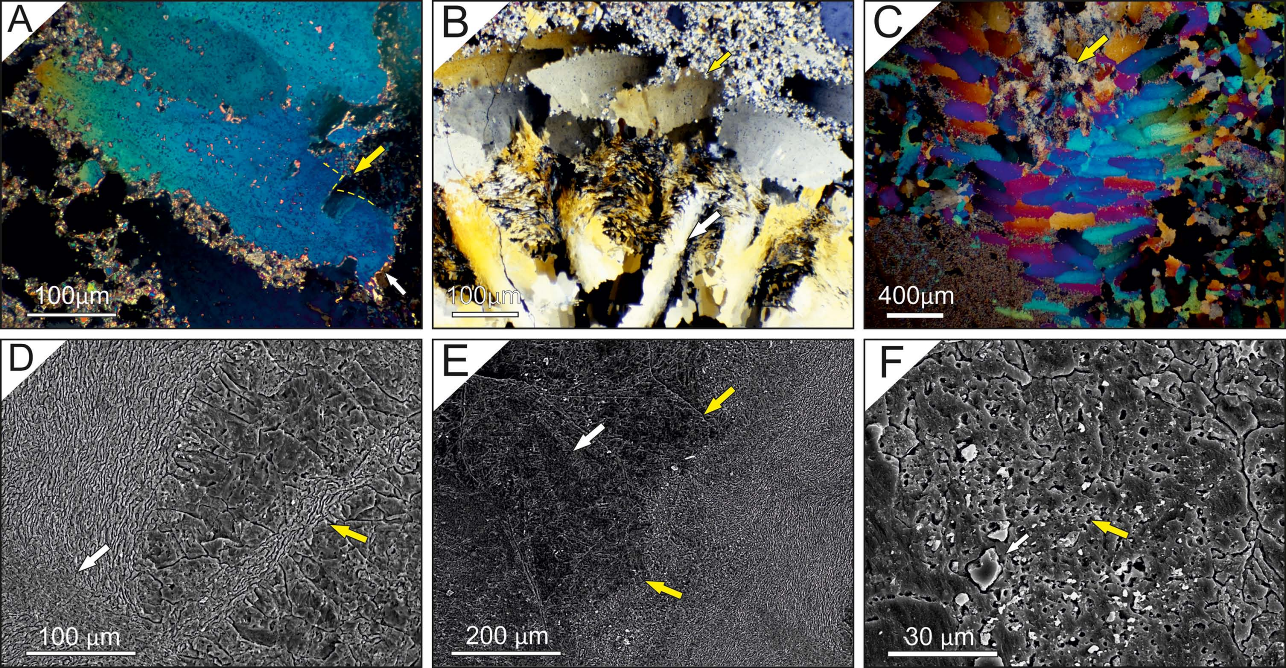
A
100µm
B
100µm
C
400µm
D
100 µm
E
200 µm
F
30 µm

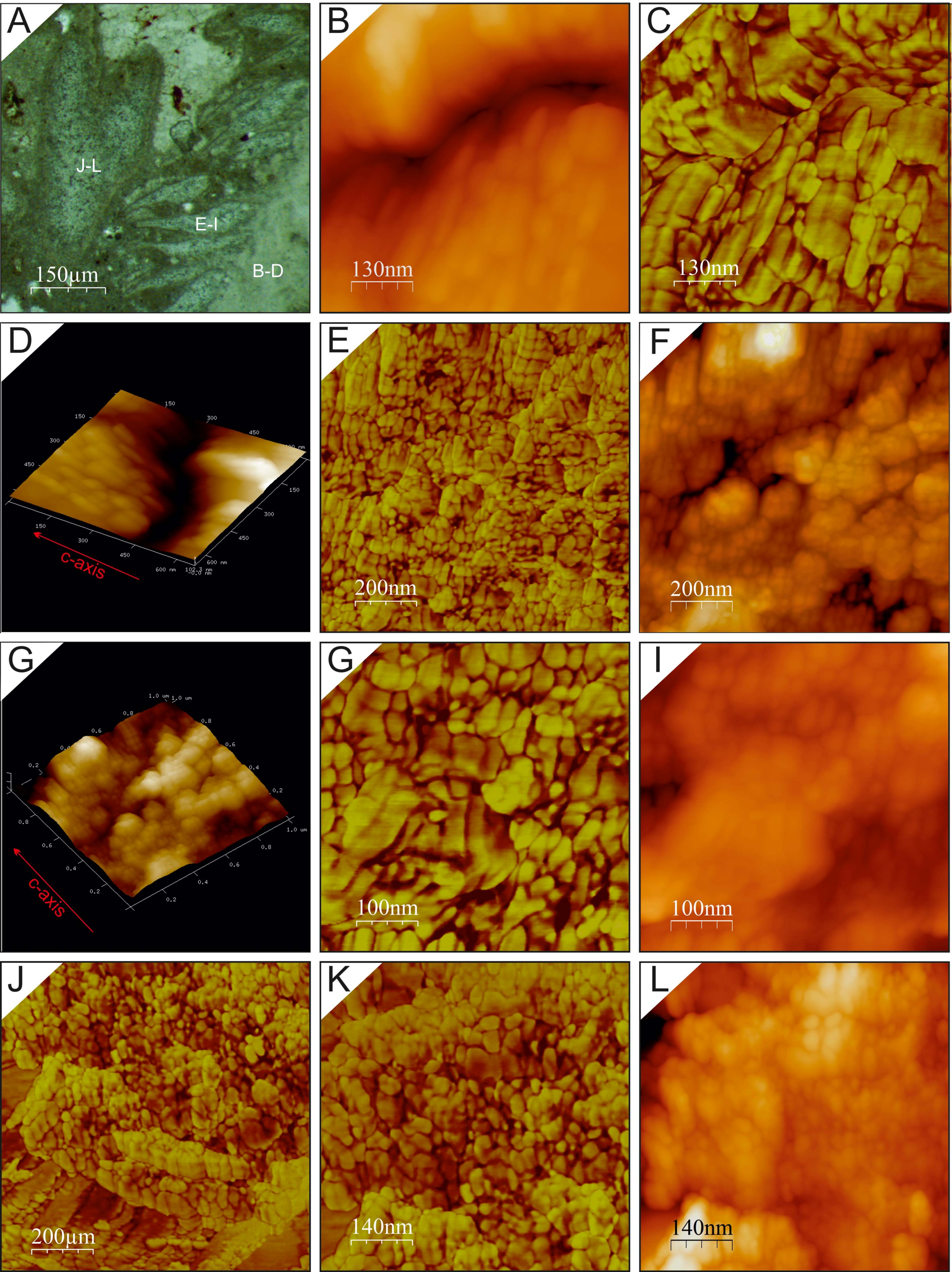
A
J-L
E-I
B-D
150μm
B
130nm
C
130nm
D
150
300
450
150
300
450
150
300
450
600 nm
150
300
450
600 nm
102.3 nm
-0.0 nm
c-axis
E
200nm
F
200nm
G
1.0 um
1.0 um
0.8
0.6
0.4
0.2
0.8
0.6
0.4
0.2
0.8
0.6
0.4
0.2
1.0 um
0.8
0.6
0.4
0.2
c-axis
G
100nm
I
100nm
J
200μm
K
140nm
L
140nm

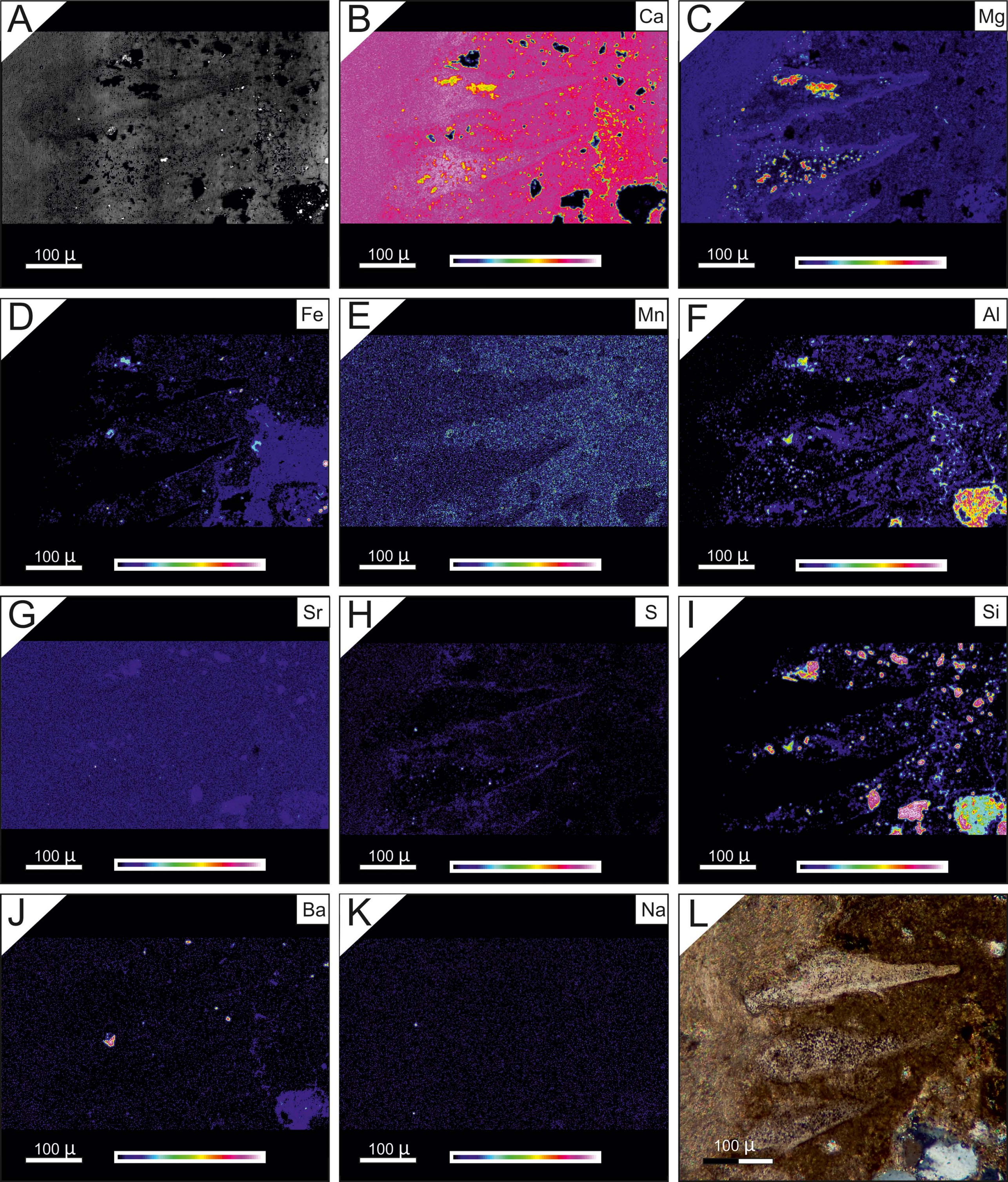
A
100 µ
B
Ca
100 µ
C
Mg
100 µ
D
Fe
100 µ
E
Mn
100 µ
F
Al
100 µ
G
Sr
100 µ
H
S
100 µ
I
Si
100 µ
J
Ba
100 µ
K
Na
100 µ
L
100 µ

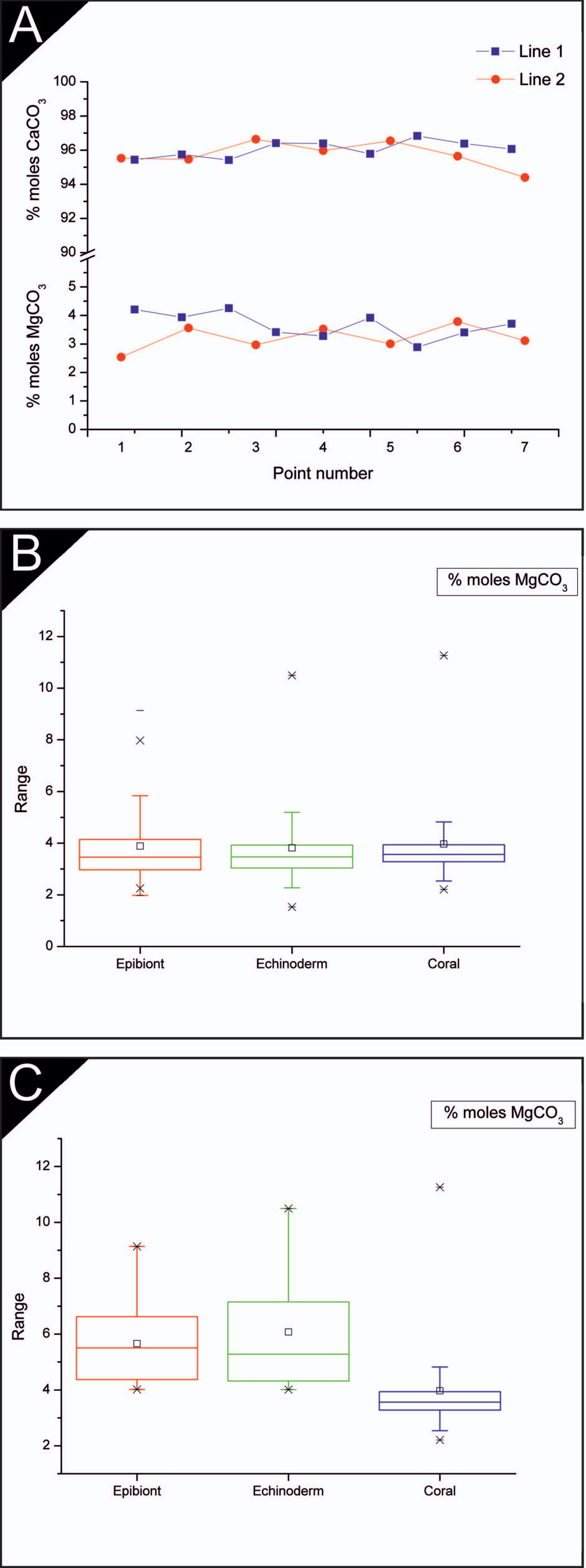
A
Line 1
Line 2
% moles $CaCO_3$
100
98
96
94
92
90
% moles $MgCO_3$
5
4
3
2
1
0
1
2
3
4
5
6
7
Point number
B
% moles $MgCO_3$
Range
12
10
8
6
4
2
0
Epibiont
Echinoderm
Coral
C
% moles $MgCO_3$
Range
12
10
8
6
4
2
Epibiont
Echinoderm
Coral

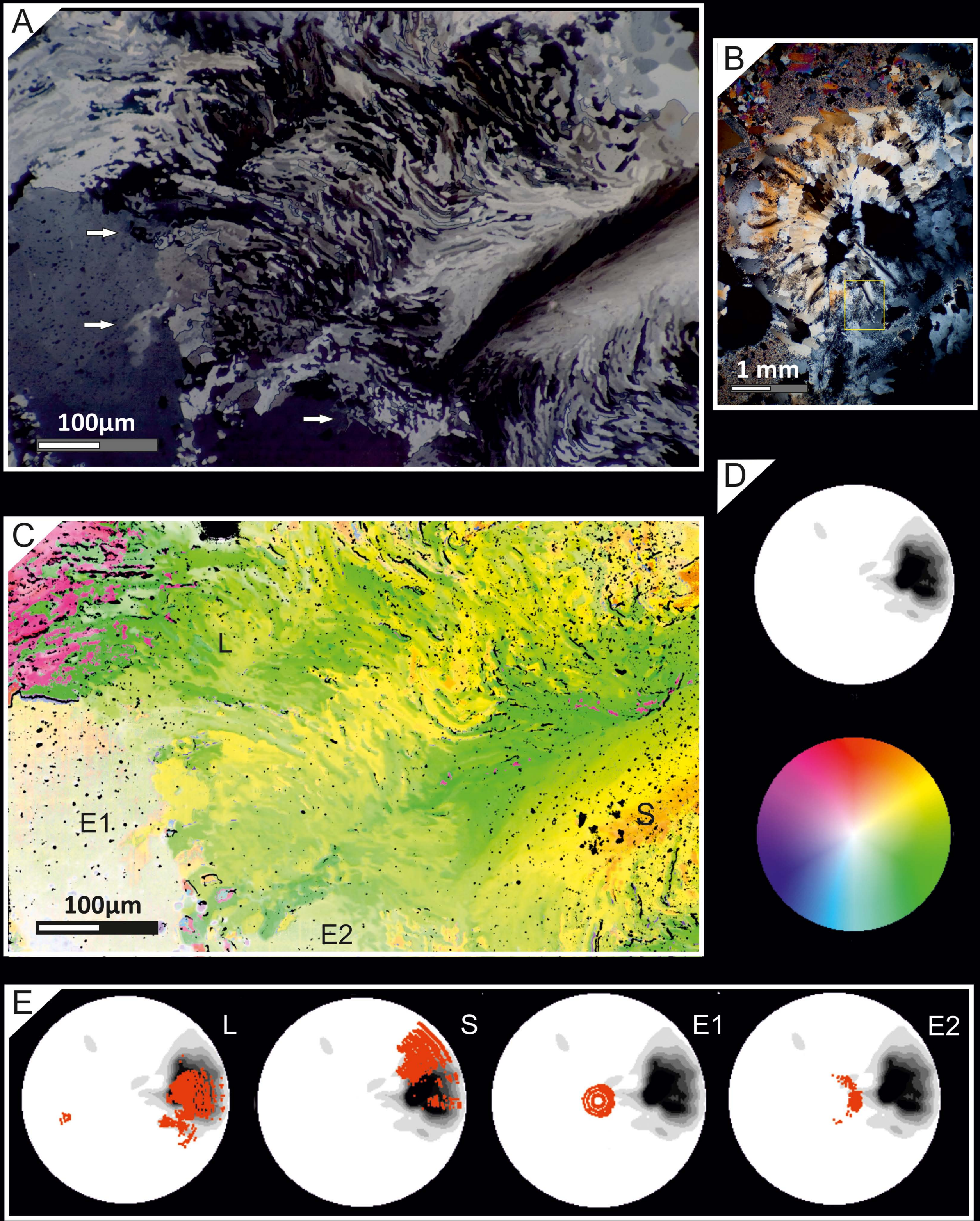
A
100µm
B
1 mm
C
L
E1
S
100µm
E2
D
E
L
S
E1
E2

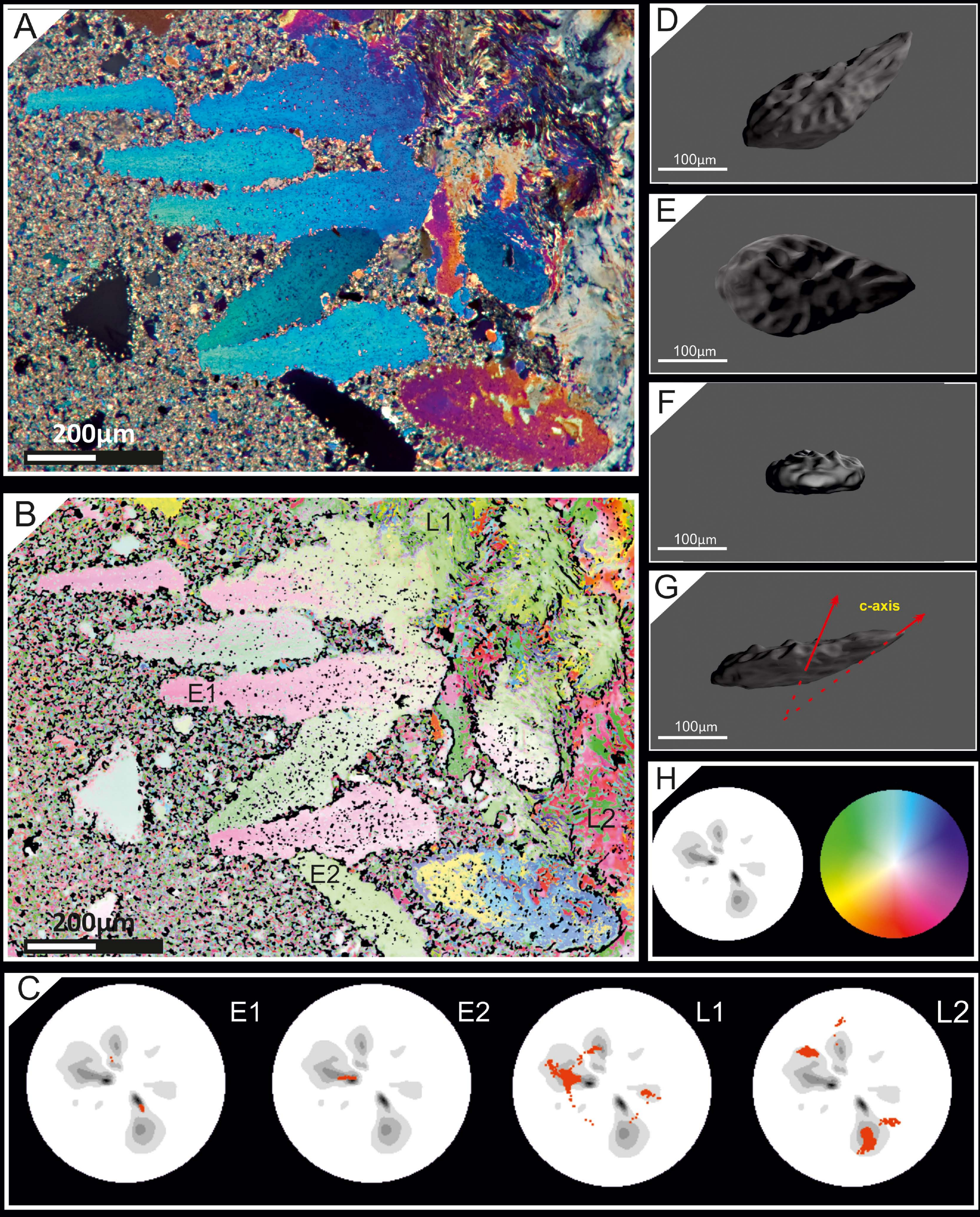
A
200µm
B
L1
E1
L2
E2
200µm
C
E1
E2
L1
L2
D
100µm
E
100µm
F
100µm
G
c-axis
100µm
H

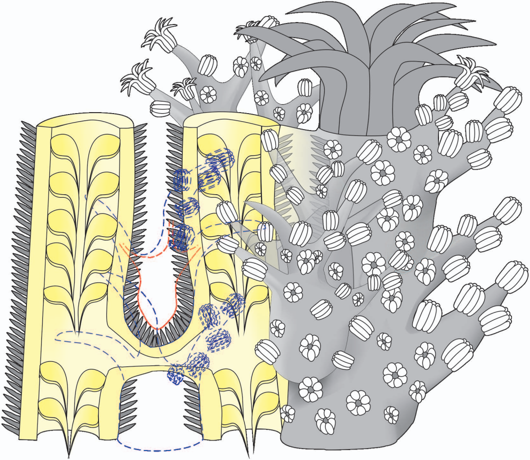

Reconstructing a Carboniferous inferred coral-alcyonarian association using a biomineralogical approach

Supporting Data

Ismael Coronado, Esperanza Fernández-Martínez, Sergio Rodríguez, Francis Tourneur

[a*] Departamento de Paleontología, Universidad Complutense de Madrid, C/José Antonio Nováis 2, Ciudad Universitaria, E-28040 Madrid, Spain. icoronad@ucm.es

[b] Departamento de Geografía y Geología, Facultad de Ciencias Biológicas y Ambientales, Universidad de León, Campus de Vegazana s/n, 24071 León, Spain. e.fernandez@unileon.es

[c] Instituto de Geociencias (IGEO. CSIC-UCM), C/José Antonio Nováis 2, Ciudad Universitaria, E-28040 Madrid, Spain. sergrodr@geo.ucm.es

[d] Pierres et Marbres de Wallonie, ASBL. 11, rue des Pieds d'Alouette. B-5100 Naninne, Belgium. francis.tourneur@pierresetmarbres.be

RELATIVE TO METHODS

Microstructural characterisation

SEM and petrographic microscopy were used for visualisation and characterisation of the microstructures in both corals and scales. Specimen DPM 00782 SYR02 was cut, polished and etched with formic acid 2% solution for 7 seconds for SEM. Images were obtained with a JEOL JSM-6400 scanning electron microscope operated to 20kV, equipped with an EDX system, located in the National Centre of Electron Microscopy (Universidad Complutense de Madrid, Spain). Four ultra-thin sections (two transverse and two longitudinal from the Morocco and Fuenteobejuna specimens) were studied using petrographic microscopy. Samples from the Los Santos de Maimona section were rejected due to the poor preservation of the fossils.

Nanostructural characterisation

To study the samples with AFM, a piece of a thin-section made from specimen DPM 00782 SYR01, and previously studied using petrographic microscopy, was cut by a circular diamond cutter. The piece of thin-section was etched with a Milli-Q water solution for 7 h and observed with an Atomic Force Microscope (model Digital Instruments Nanoscope IIIA (Veeco), located at the National Centre of Electron Microscopy (Universidad Complutense de Madrid, Spain)). The images were obtained at room temperature and in air using a tapping mode with a silica tip. The images were processed with Nanoscope software v5.30 r3 sr3 of Veeco Instruments Inc. and WSxM v5.0 Develop 5.0 software of Nanotec (Horcas *et al*., 2007). AFM images have a resolution very similar to TEM, but without thinning, and so artefacts are reduced. Two main types of images can be obtained with AFM: height and phase. Height images enable topographical reconstruction of the crystal surface, while phase images provide information regarding the variations in material properties. More details concerning the properties of each image could be found in Coronado *et al*. (2013).

Chemical characterisation

Electron microprobe analysis was conducted on thin sections, with a JEOL JZA-8900 with 4 detectors, located at the National Centre of Electron Microscopy (the Universidad Complutense of Madrid, Spain). A quantification of some major, minor and trace elements (MTE) was made with EMPA in corals, scales and echinoderm plates to check for similarities and differences. Eight elements were analysed (Ca^{2+}, Mg^{2+}, Sr^{2+}, S^{6+}, Ba^{2+}, Na^{+}, Mn^{2+} and Fe^{2+}) at each point. Transverse sections were made in the walls of the corallites and scales. The points in the sections were separated by 50 µm (with a 5 µm spot size) in the corals and at selected points in the scales. In addition, ten elements (Ca^{2+}, Mg^{2+}, Sr^{2+}, S^{6+}, Ba^{2+}, Na^{+}, Mn^{2+}, Fe^{2+}, Al^{2+} and Si^{2+}) were mapped at the contact points between some of the scales and the coral wall. The EMPA mapping enables simultaneous analysis of different elements and the generation of distribution maps for each element with 1-µm resolution.

The cathodoluminescence study was carried out with a cold CL probe 8200 MK 4 system made by Cambridge Image Technology Ltd (Cambridge, UK), working at 16 kV and a current of 0.5 mA, fitted to a petrographic microscope Nikon Eclipse E400 POL with camera, located in the Geological Storage Division, Hidrogeochemical Group, Ciemat (Madrid, Spain). CL microscopy has been applied in the past with the aim to provide the preservation state of Palaeozoic coral microstructures (e.g. Mas and Rodríguez 1990; Fedorowski 2003; Coronado et al., 2013; Coronado et al., 2014a).

Crystallographic characterisation

For CIP analysis, two ultra-thin sections (transverse and longitudinal) of specimen DPM 00782 SYR01 were used. The CIP method (computer-integrated-polarisation microscopy) has been described by Heilbronner *et al.* (1993), Heilbronner (2000), and Heilbronner &Barret (2014) as a method for texture analysis and optical orientation imaging. It determines the c-axis orientations of uniaxial minerals from optical micrographs and displays the results in the form of pole figures and orientation images, using a colour-code (CLUT), which represents each orientation. Studies of structural geology in quartz and calcites (van Daalen *et al.*, 1999; Trullenque *et al.*, 2006) have had good results with this method. This method has been applied to biomineralisation studies of recent and fossil specimens (Coronado *et al.*, in press A), and the results suggest that it can be a powerful tool that can supplement and correlate with EBSD data. It also allows us to obtain crystallographic, structural and diagenetic information quickly by the use of ultra-thin sections in calcite fossil samples (e.g., tabulate corals). One advantage of this technique in biomineralisation studies is the quick processing of data at different scales, working easily at 4x to 40x magnifications, covering large areas, quickly and with low cost.

Three CIP analyses were performed with a petrographic Zeiss and a Kodak Wratten nº25 filter, at 20x and 4x magnifications, to determine the crystallographic correlation between the scales and the coral wall microstructure and processes with Image SXM software (Barret, 1997).

Fig. 1

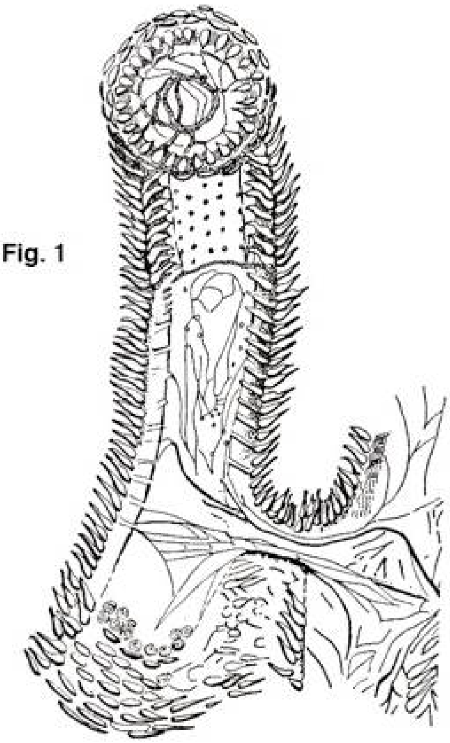

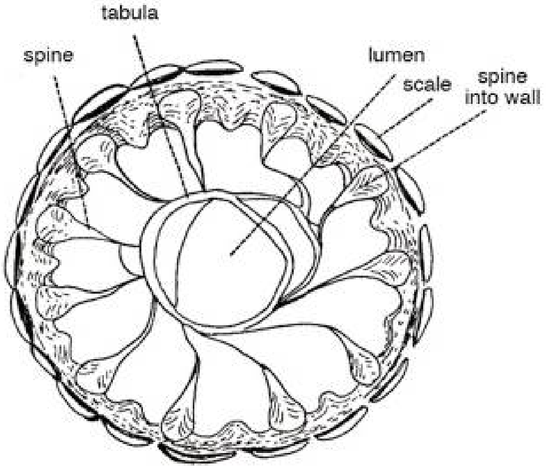

Fig. 2a

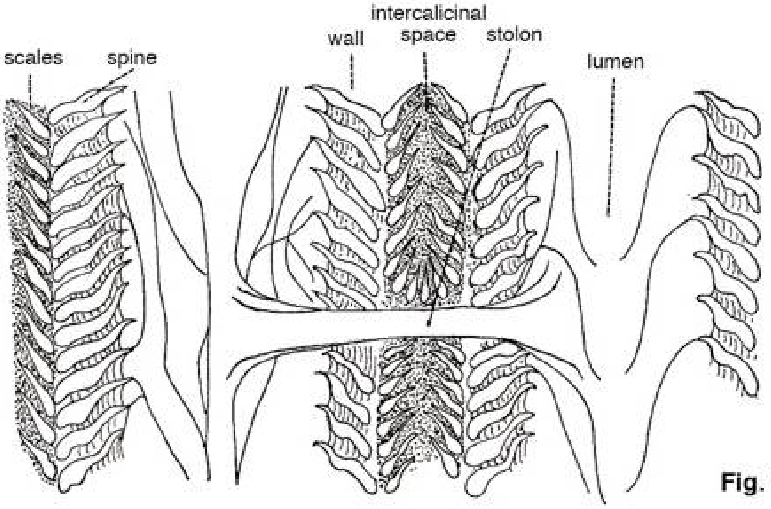

Fig. 2b

Fig. S1 Drawings of *Syringoalcyon* after Termier and Termier (1975), Fig 1). Reconstruction of a whole corallite surrounded by scales. Fig 2a) Transverse section of a corallite. Fig. 2b)

Longitudinal section of two corallites (note the occurrence of spines growing in the coral wall) and the arrangement of the scales in the intercalcinal space.

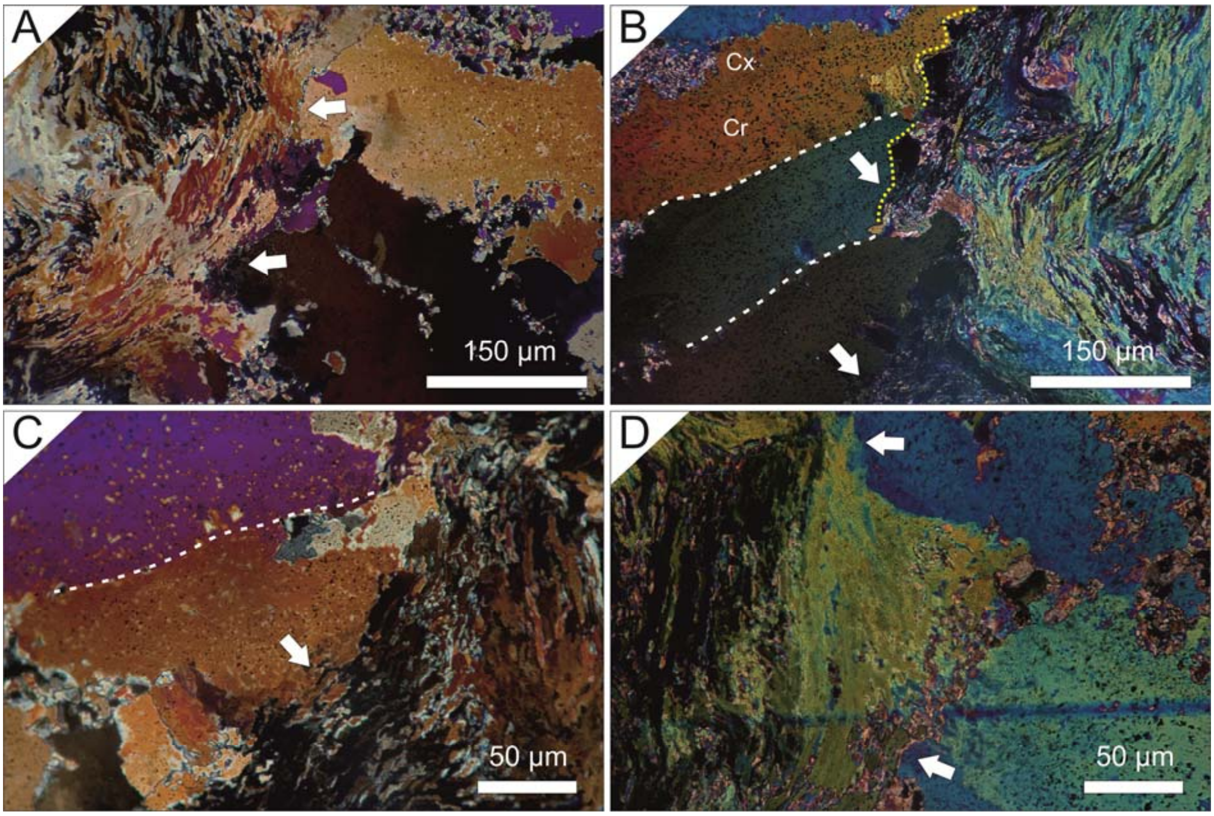

Fig. S2. A-D) Petrographic images of the insertion area between the longitudinal section of coral wall and scales. Specimen DPM 00782 SYR01. Note that, in the insertion areas (white arrows), the lamellae are truncated, broken or embedded in the edge of scale C). Note the footstep-shaped region in some longitudinal sections of scales B). Note the difference of turbid inclusion between the cortex (Cx) and the core (Cr). Dashed white line delimits the contact area between two adjacent scales.

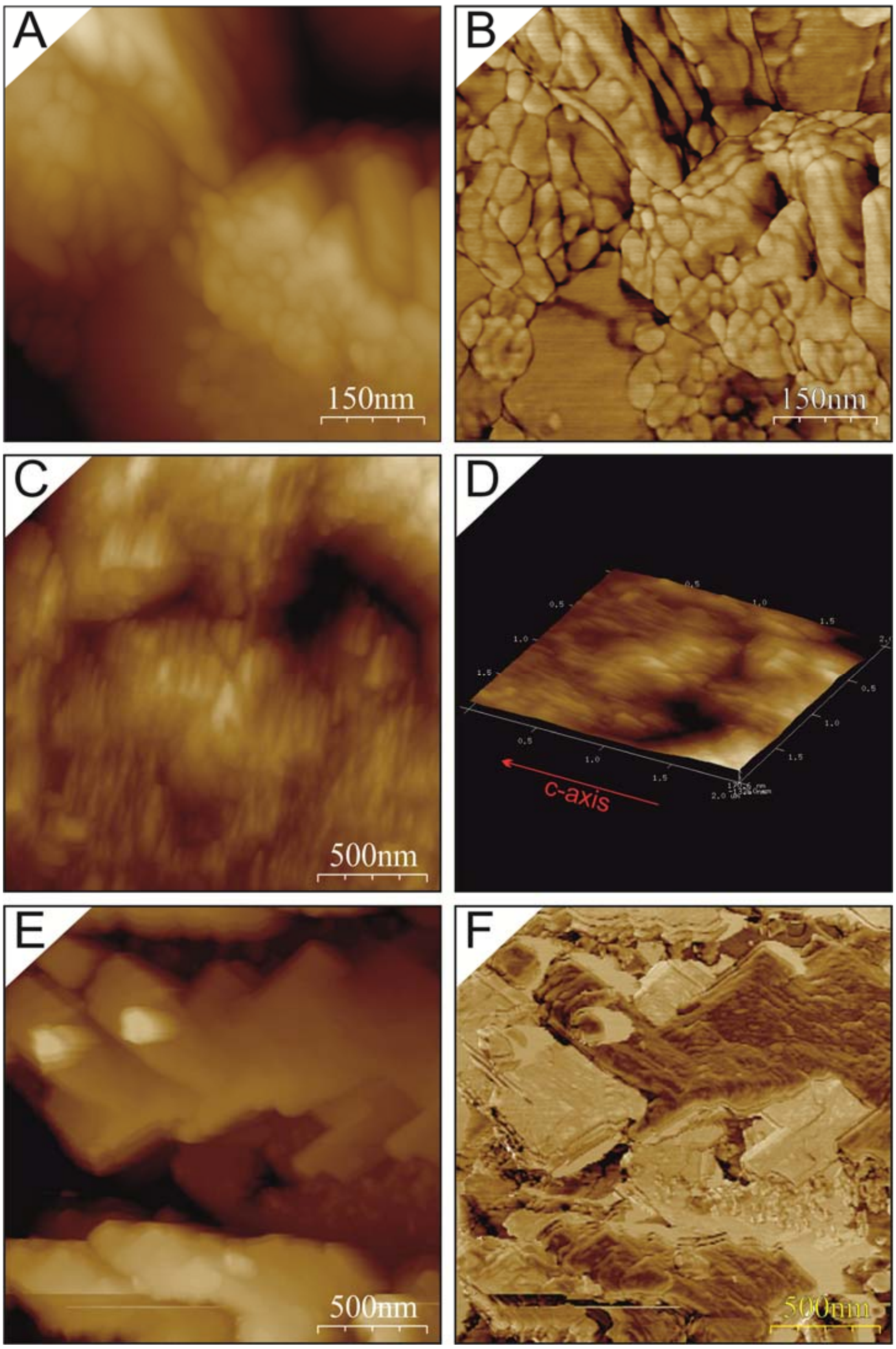

Fig. S3 AFM images of scales of sample DPM 00782 SYR01. A-B) Height and phase images of the longitudinal section of a scale. Note the nanocrystals that are partially merged and the flat region with the nanotexture has been completely obliterated. C) Height image of medium magnification where nanofibres co-oriented in the same direction are observed; they clearly show that the scales are a biocomposite. D) Three-dimensional AFM image of the nanofibres of a scale. The red arrow shows the direction of the c-axis. E-F) AFM images of a echinoderm ossicle. E-F) Height and phase images where the nanogranules are totally obliterated and some flat regions with rhombohedral dolomite crystals can be observed.

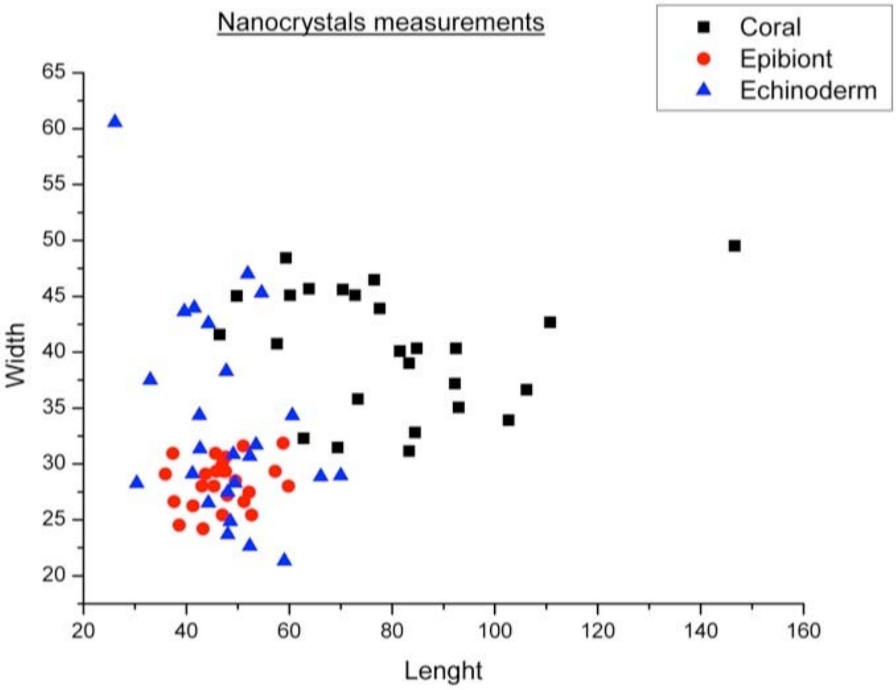

Fig. S4 Scatter diagram representing the variation of length versus width of nanocrystals measured in the three elements studied (coral wall, scales and echinoderm plates in sample DPM 00782 SYR01). Note the minor dispersion showed by the nanocrystals belong to the epibiont versus the nanocrystals from the echinoderm.

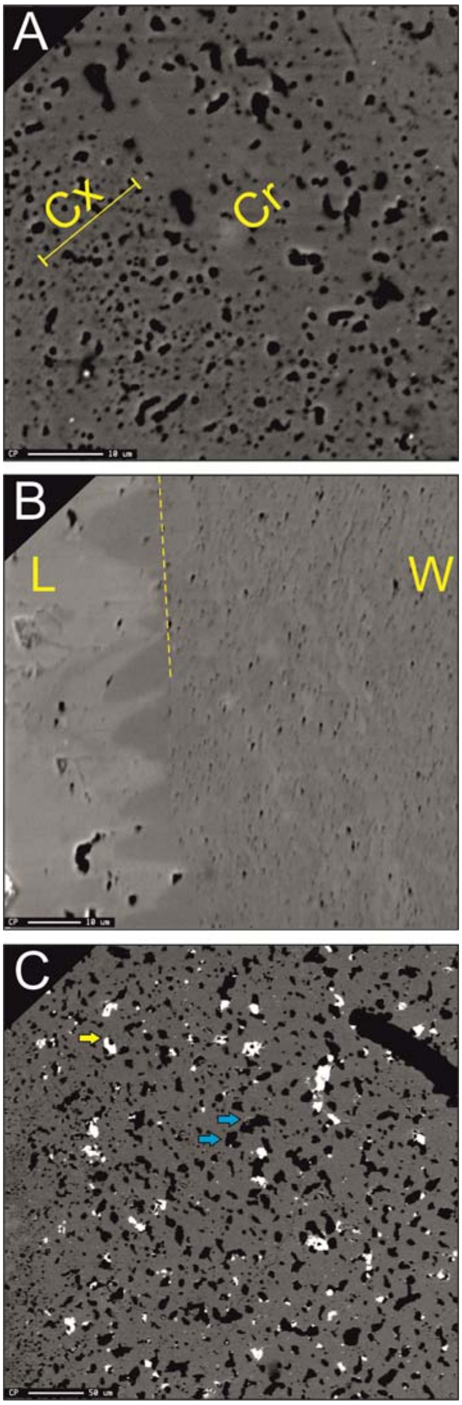

Fig. S5 BSE images of the different elements analysed by EMPA. A) Inner microstructure of a scale. Note the variation in size between the impurities (dark spots) from the cortex (“Cx”) and from the core (“Cr”). B) Coral wall (W) region in contact (yellow dash line) with the calcitic cement of the lumen (L). Note the colour variation between the cement of the lumen and the coral wall, and internally the lamellae. C) Echinoderm plate microstructure. Yellow arrow points to white crystals of celestine and blue arrows point to dark angular crystals of dolomite.

Table S1 Mean chemical compositions of skeletal elements studied by punctual analysis.

		N	Mean	S.D	Sum	Minimum	Median	Maximum	D.L. (ppm)
Coral	**mol % $SrCO_3$**	58	0.17373	0.07706	10.07606	0.02574	0.16171	0.43404	102.78
	mol % $MnCO_3$	58	0.07823	0.12202	4.53749	0	0.03693	0.65912	268.75
	mol % $CaCO_3$	58	95.46825	1.60599	5537.158	88.3583	95.96989	96.83302	97.39
	mol % $MgCO_3$	58	3.97277	1.6038	230.4206	2.20858	3.56222	11.26245	73.5
	mol % $FeCO_3$	58	0.30703	0.48864	17.80751	0	0.14391	2.82031	242.35
	S (ppm)	58	388.485	322.50711	22532.13	0	288.36	1662.075	67.37
	Na (ppm)	58	81.07548	103.64135	4702.378	0	22.251	437.603	81.52
	Ba (ppm)	58	176.3602	344.77544	10228.89	0	0	1666.002	305.29
Epibiont	**mol % $SrCO_3$**	113	0.19218	0.06762	21.71601	0	0.18273	0.38682	102.78
	mol % $MnCO_3$	113	0.06487	0.11421	7.33052	0	0.0367	0.8751	268.75
	mol % $CaCO_3$	113	95.53737	1.43137	10795.72	90.423	95.94499	97.38671	97.39
	mol % $MgCO_3$	113	3.88709	1.4217	439.2416	1.97683	3.45489	9.13789	73.5
	mol % $FeCO_3$	113	0.31849	0.5335	35.98895	0.01003	0.15589	3.79789	242.35
	S (ppm)	113	453.8764	387.50443	51288.03	0	364.455	2435.04	67.37
	Na (ppm)	113	64.78388	84.46812	7320.579	0	22.251	385.684	81.52
	Ba (ppm)	113	241.9183	312.50289	27336.76	0	62.699	1522.69	305.29
Echinoderm	**mol % $SrCO_3$**	88	0.17935	0.06879	15.78258	0.05803	0.17111	0.32513	102.78
	mol % $MnCO_3$	88	0.05714	0.07986	5.02813	0	0.03289	0.5418	268.75
	mol % $CaCO_3$	88	95.72524	1.47437	8423.821	89.28435	96.16275	97.98245	97.39
	mol % $MgCO_3$	88	3.8172	1.48374	335.9133	1.5336	3.48181	10.49506	73.5
	mol % $FeCO_3$	88	0.22108	0.29885	19.45475	0	0.13945	1.77562	242.35
	S (ppm)	88	400.5	413.31893	35244	16.02	304.38	2791.485	67.37
	Na (ppm)	88	70.71435	79.04763	6222.863	0	48.2105	304.097	81.52
	Ba (ppm)	88	228.8106	299.73674	20135.34	0	49.2635	1218.152	305.29

Table S2 Mean chemical compositions of HMC skeletal elements studied by punctual analysis.

		N	Mean	S.D	Sum	Minimum	Median	Maximum	D.L. (ppm)
Epibiont	**mol % $SrCO_3$**	33	0.17284	0.04652	5.70364	0.08425	0.16547	0.27643	102.78
	mol % $MnCO_3$	33	0.0483	0.05011	1.59404	0	0.04862	0.22304	268.75
	mol % $CaCO_3$	33	93.8795	1.30681	3098.023	90.423	94.01872	95.68416	97.39
	mol % $MgCO_3$	33	5.66161	1.37733	186.833	4.01698	5.5056	9.13789	73.5
	mol % $FeCO_3$	33	0.23775	0.34011	7.84581	0.01452	0.12377	1.8038	242.35
	S (ppm)	33	755.3673	515.0796	24927.12	168.21	576.72	2435.04	67.37
	Na (ppm)	33	49.22191	74.83497	1624.323	0	0	252.178	81.52
	Ba (ppm)	33	258.6673	267.7731	8536.021	0	259.753	922.571	305.29
Echinoderm	**mol % $SrCO_3$**	17	0.16173	0.06147	2.74938	0.05912	0.15116	0.30372	102.78
	mol % $MnCO_3$	17	0.04098	0.05675	0.69674	0	0.0114	0.18938	268.75
	mol % $CaCO_3$	17	93.54475	2.0658	1590.261	89.28435	94.2852	95.74372	97.39
	mol % $MgCO_3$	17	6.07315	2.06537	103.2435	4.01317	5.27848	10.49506	73.5
	mol % $FeCO_3$	17	0.17939	0.12355	3.0497	0	0.2125	0.46823	242.35
	S (ppm)	17	839.4009	725.1319	14269.82	72.09	644.805	2791.485	67.37
	Na (ppm)	17	94.23953	99.70848	1602.072	0	66.753	304.097	81.52
	Ba (ppm)	17	110.1184	215.8935	1872.013	0	0	689.689	305.29

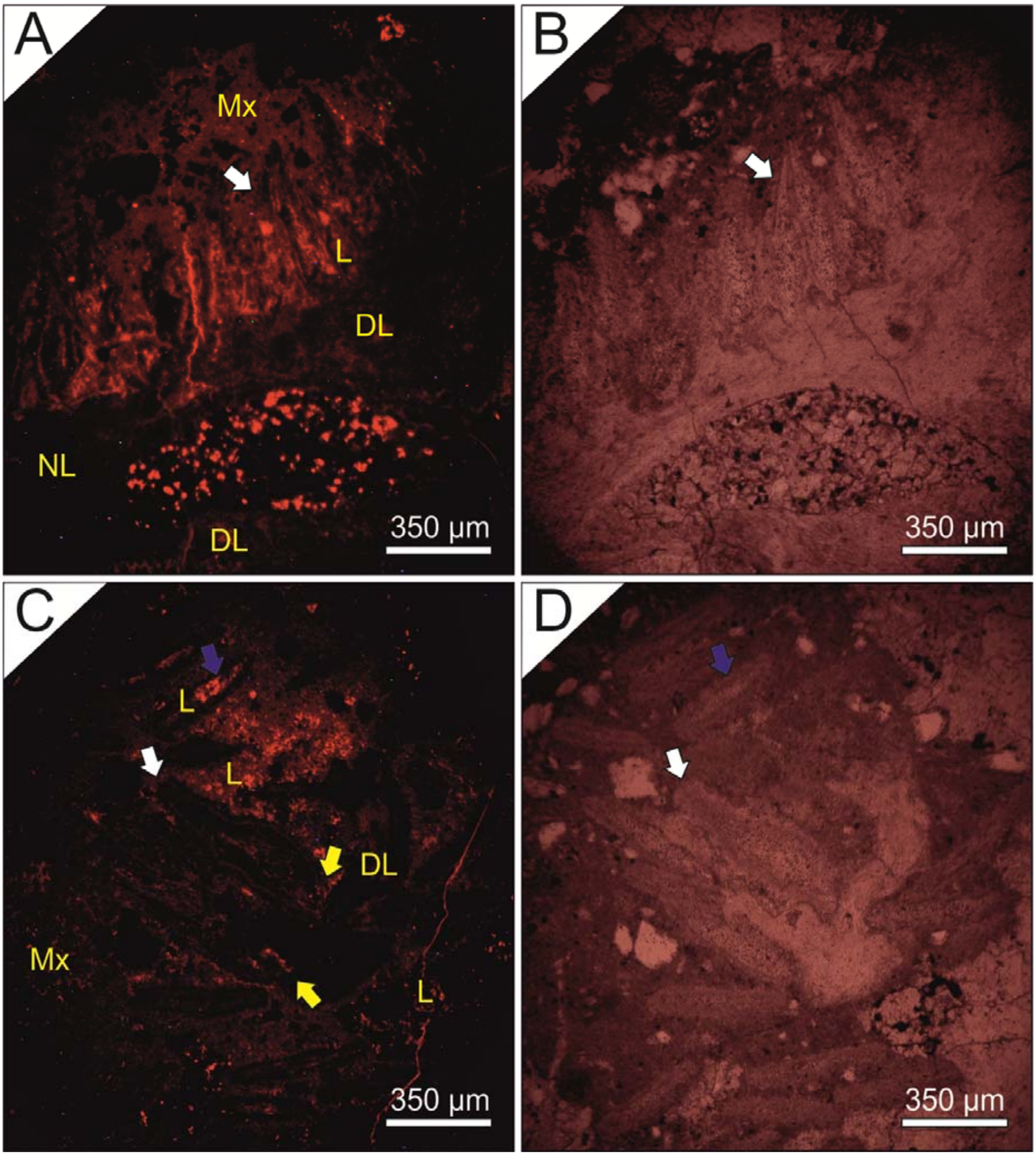

Fig. S6 A-D) Cathodoluminescence and petrographic images of a longitudinal section of *Syringoalcyon* where the scales growing over a stolon can be observed. Specimen DPM 00782 SYR01. Note the high luminescence of scales regarding to the coral wall. White arrow points to the apex of a scale as benchmark. C-D) Cathodoluminescence and petrographic images of an oblique section of *Syringoalcyon*. Note the null luminescence regarding to the insertion areas (yellow arrows). White arrows point to the apex of a scale as benchmark. Blue arrows point to the microdolomite crystals. NL = non-luminescent calcite. DL = Dull-luminescent calcite. L = Luminescent calcite. Mx = Matrix.

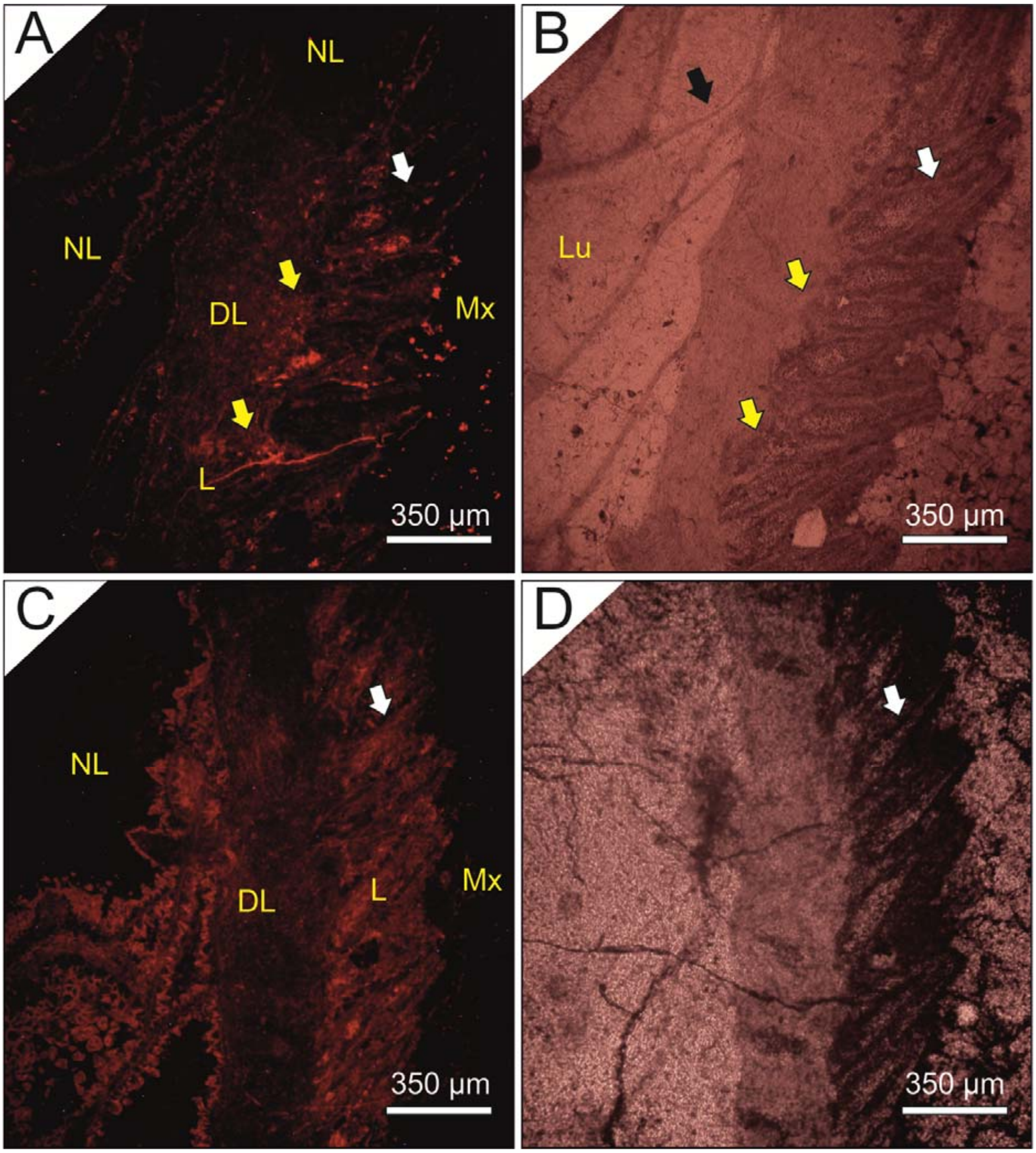

Fig. S7 A-D) Cathodoluminescence images of two longitudinal sections of *Syringoalcyon*. Specimen DPM 00782 SYR01. White arrow points to the fringe of a scale as benchmark. Yellow arrows point to the luminescent insertion areas. NL = non-luminescent calcite. DL = Dull-luminescent calcite. L = Luminescent calcite. Mx = Matrix. Lu = Lumen.

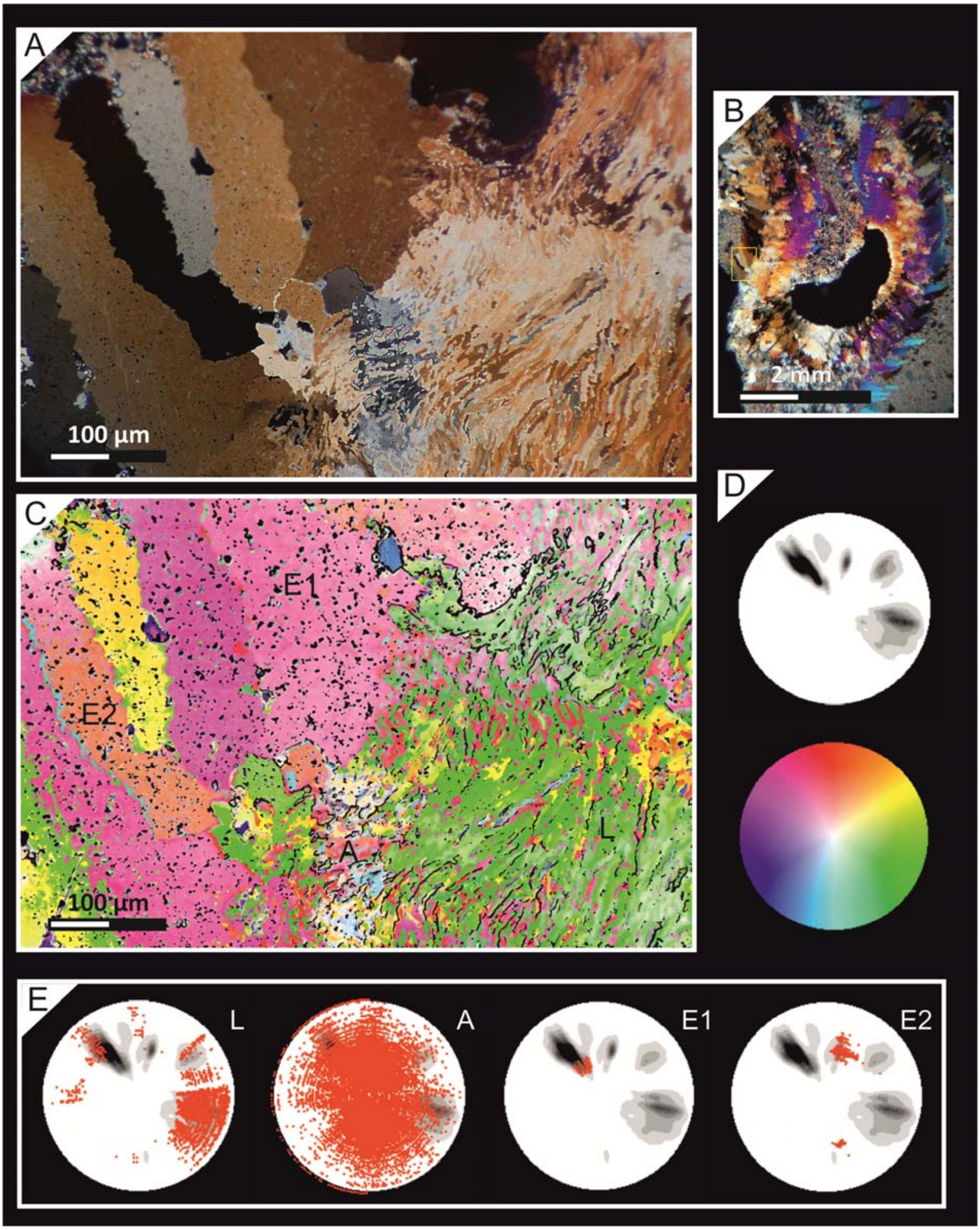

Fig. S8 Specimen DPM 00782 SYR01. CIP images and derived *c*-axis pole figures of a longitudinal section of *Syringopora* close to the area where the scales are inserted. A-B) Ultra-thin section image of the investigated area. A) Large magnification. B) Yellow frame shows the investigated area and its position in relation to the coral wall. C) Orientation image.

Black regions correspond to the thick regions of contact between crystals and opaque impurities and they were considered for the *c*-axis pole figure calculation. D) Pole figure of the entire area calculated as an orientation distribution function, provided in multiples of uniform distribution intervals of 0.5 for c axis orientations. Standard colour look-up table (CLUT) in the lower region. E) Pole figures of different areas of detailed study superimposed on the whole pole figure. Red points correspond to the punctual *c*-axis orientation of each pixel. L-region corresponds to the lamellar zone. A-region corresponds to diagenetic alteration and a random distribution can be seen. E1 and E2-regions belong to different epibiont scales.

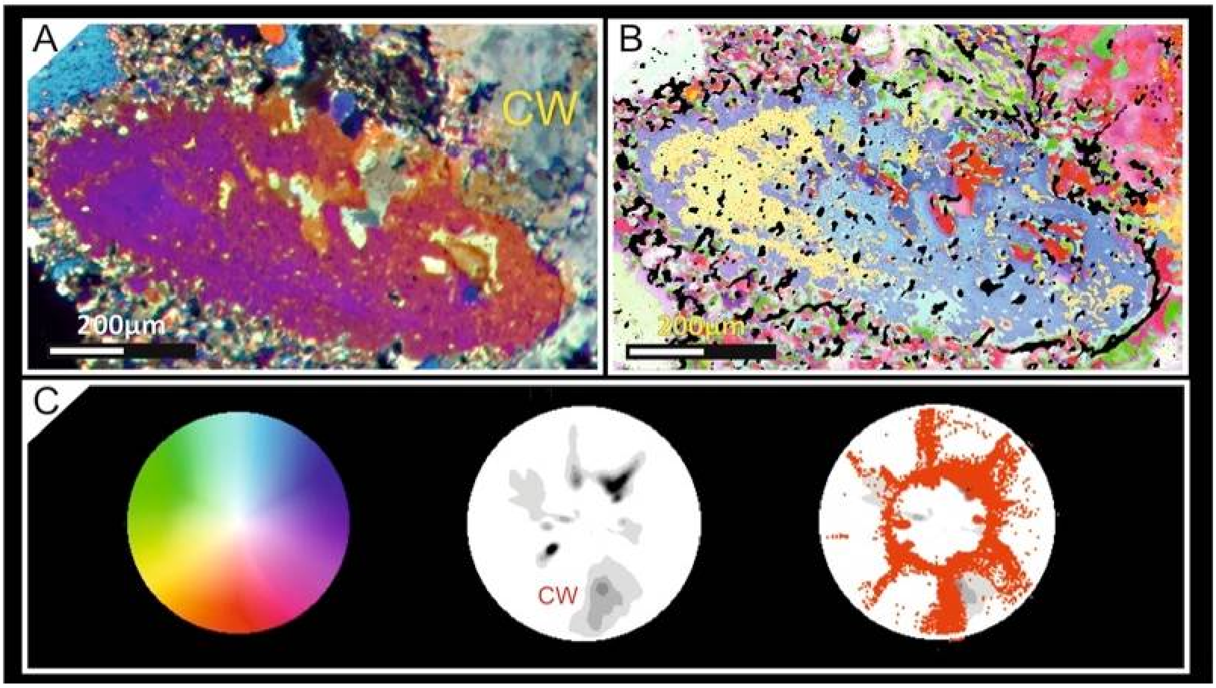

Fig. S9 Specimen DPM 00782 SYR01. CIP images and the derived c-axis pole figures of the transverse section of a scale just in the contact with the coral wall. A) Ultra-thin section image of the investigated area. The portion on the right belongs to the coral wall. B) Orientation image of the studied area. Black regions belong to regions of thick contact between the crystals and opaque impurities and they were not considered for the c-axis pole figure calculation. C) Pole figure of the whole area calculated as an orientation distribution function, given in multiples of uniform distribution intervals of 0.5 for c-axis orientations. Standard colour look-up table (CLUT) in the lower region. Cw shows the main orientation that belongs to the coral wall. The right pole figure represents the orientations of the scale superimposed on the whole pole figure. The red points correspond to the punctual c-axis orientation of each pixel. Note the random orientations of the inner parts of the scale.

REFERENCES

Coronado I, Pérez-Huerta A, Rodríguez S (2013) Primary biogenic skeletal structures in Multithecopora (Tabulata, Pennsylvanian). Palaeogeography, Palaeoclimatology, Palaeoecology, 386, 286-299.

Coronado I, Pérez-Huerta A, Rodríguez S (2014) Computer-integrated polarisation (CIP) in the analysis of fossils: a case of study in a Palaeozoic coral (Sinopora, Syringoporicae, Carboniferous). *Historical Biology*, 1-15.

Fedorowski J (2003) Some remarks on diagenesis of rugose coral skeletons. *Geologos,* **6**, 89-109.

Heilbronner R (2000) Automatic grain boundary detection and grain size analysis using polarization micrographs or orientation images. Journal of Structural Geology, 22, 969-981.

Heilbronner R, Barret S (2014) Image Analysis in Earth Sciences - Microstructures and Textures of Earth Materials, Springer, London.

Heilbronner RP, Pauli C (1993) Integrated spatial and orientation analysis of quartz c-axes by computer-aided microscopy. Journal of Structural Geology, 15, 369-382.

Horcas I, Fernández R, Gómez-Rodríguez JM, Colchero J, Gómez-Herrero J, Baro A (2007) WSXM: a software for scanning probe microscopy and a tool for nanotechnology. Review of Scientific Instruments, 78, 8.

Mas R, Rodríguez S (1990) Cathodoluminiscence as a tool in fosildiagenetic analyses of Late Paleozoic Corals. In: *Comunicaciones de la Reunión de Tafonomía y Fosilización : Madrid 20-22 de septiembre de 1990* (ed López SF), Madrid.

Ries JB (2006) Mg fractionation in crustose coralline algae: Geochemical, biological, and sedimentological implications of secular variation in the Mg/Ca ratio of seawater. Geochimica et Cosmochimica Acta, 70, 891-900.

Stanley SM (2006) Influence of seawater chemistry on biomineralization throughout phanerozoic time: Paleontological and experimental evidence. Palaeogeography, Palaeoclimatology, Palaeoecology, 232, 214-236.

Trullenque G, Kunze K, Heilbronner R, Stünitz H, Schmid SM (2006) Microfabrics of calcite ultramylonites as records of coaxial and non-coaxial deformation kinematics: Examples from the Rocher de l'Yret shear zone (Western Alps). Tectonophysics, 424, 69-97.

Van Daalen M, Heilbronner R, Kunze K (1999) Orientation analysis of localized shear deformation in quartz fibres at the brittle–ductile transition. Tectonophysics, 303, 83-107.